



PAPER

Emergent anomalous transport and non-Gaussianity in a simple mobile-immobile model: the role of advection

OPEN ACCESS

RECEIVED
23 January 2023REVISED
20 May 2023ACCEPTED FOR PUBLICATION
26 May 2023PUBLISHED
9 June 2023Original Content from
this work may be used
under the terms of the
[Creative Commons
Attribution 4.0 licence](#).Any further distribution
of this work must
maintain attribution to
the author(s) and the title
of the work, journal
citation and DOI.Timo J Doerries¹, Ralf Metzler^{1,2,*}  and Aleksei V Chechkin^{1,3,4} ¹ Institute of Physics & Astronomy, University of Potsdam, 14476 Potsdam, Germany² Asia Pacific Centre for Theoretical Physics, Pohang 37673, Republic of Korea³ Faculty of Pure and Applied Mathematics, Hugo Steinhaus Centre, Wrocław University of Science and Technology, Wyspianskiego 27, 50-370 Wrocław, Poland⁴ Akhiezer Institute for Theoretical Physics, 61108 Kharkov, Ukraine

* Author to whom any correspondence should be addressed.

E-mail: rmetzler@uni-potsdam.de

Keywords: diffusion, drift/advection, non-Gaussianity

Abstract

We analyse the transport of diffusive particles that switch between mobile and immobile states with finite rates. We focus on the effect of advection on the density functions and mean squared displacements (MSDs). At relevant intermediate time scales we find strong anomalous diffusion with cubic scaling in time of the MSD for high Péclet numbers. The cubic scaling exists for short and long mean residence times in the immobile state τ_{im} . For long τ_{im} the plateau in the MSD at intermediate times, previously found in the absence of advection, also exists for high Péclet numbers. Initially immobile tracers are subject to the newly observed regime of advection induced subdiffusion for short immobilisations and high Péclet numbers. In the long-time limit the effective advection velocity is reduced compared to advection in the mobile phase. In contrast, the MSD is enhanced by advection. We explore physical mechanisms behind the emerging non-Gaussian density functions and the features of the MSD.

1. Introduction

One of the simplest equations to describe the transport of tracers in subsurface aquifers (water-bearing layers or permeable rock or sediment) is the advection–diffusion equation [1, 2]

$$\frac{\partial}{\partial t} G(x, t) = D \frac{\partial^2}{\partial x^2} G(x, t) - v \frac{\partial}{\partial x} G(x, t), \quad (1)$$

where $G(x, t)$ denotes the probability density function of a tracer particle, v the constant advection velocity, and D the diffusion constant. The initial condition is $G(x, 0) = \delta(x)$, corresponding to a ‘point injection’ in geoscience. The probability density function encoded by equation (1) with initial condition $G(x, 0)$ is given by the Gaussian

$$G(x, t) = \frac{1}{\sqrt{4\pi Dt}} \exp\left(-\frac{(x - vt)^2}{4Dt}\right), \quad (2)$$

with similarity variable $x - vt$, where the first moment $\langle x(t) \rangle = \int_{-\infty}^{\infty} xG(x, t)dx = vt$ and the mean squared displacement (MSD) $\langle [x(t) - \langle x(t) \rangle]^2 \rangle = 2Dt$ are linear at all times. The latter does not depend on v . The alternatively used mobile-immobile model (MIM) is a more elaborate model that takes pores into account, where a tracer can remain immobile for an exponentially random duration [3–5]. This linear first order mass transfer is often used to model sorbing solutes, as well [6–8]. In an MIM the concentration is split into a mobile density $n_{\text{m}}(x, t)$ and an immobile density $n_{\text{im}}(x, t)$. In the mobile state tracers are subject to advection and diffusion in the same way as in the advection–diffusion equation (1). MIMs have been used extensively in geophysical systems [3, 4, 8–18]. Apart from geophysical applications, we mention two other applications,

where motion interrupted by transient immobilisations has been studied. The first application pose biological systems, such as potassium channels in the membrane of living cells [19] and transcription factors [20]. Many systems such as tau proteins [21, 22], synaptic vesicles [23], complexes at the endoplasmic reticulum [24], the drug molecule doxorubicin in silica nanoslits [25] and DNA binding proteins [26–35] may be described in terms of an MIM, in which the residence times in the immobile state are distributed exponentially⁵. The corresponding experiments were conducted in flow cells [26, 32–35] or occur in live biological cells [27–30]. In such cellular systems advection may arise due to the action of molecular motors causing streaming in the cytoplasm [36]. Further examples of systems with advection, where in addition immobilisations occur, include DNA molecules in microfluidic setups and bio sensors [37, 38]. The second application, featuring transient immobilisations concerns charge carriers in semiconductors, where a recent focus lies on exciton diffusion in layered perovskites and transition metal dichalcogenides [39–42]. Often, MIMs are not formulated in terms of mean residence times but with a single rate for mass exchange and a solute capacity coefficient that takes different volumes of the mobile and immobile volume into account [3, 7, 11, 12, 43]. The moments for mobile, immobile and total density of the MIM have been calculated for various initial conditions while including effects of advection and diffusion [6, 7, 13]. We here focus on the densities and MSDs at relevant intermediate time scales and unveil interesting new properties in the transport dynamics. In the short time limit initially mobile tracers behave like free Brownian tracers (2) with an MSD $\sim 2Dt$. At long times the MSD is linear, with the effective diffusivity D_{eff} containing a term proportional to v^2 , that can yield $D_{\text{eff}} > D$ [7, 13]. This is in contrast to the solution (2) of the advection-dispersion equation (1), in which the MSD does not depend on v . Below we provide a physical explanation for how this enhanced effective diffusion coefficient is brought about. Another model often used to describe the motion of tracers with immobile periods is the continuous time random walk (CTRW) [39, 44, 45], for which it was shown that exponential tails emerge in the position density [46] when a drift is present [13, 18, 47–50]. CTRWs have also been analysed for systems with two states, characterised by two waiting time distributions, such that a specific distribution is chosen alternatingly or randomly [51, 52]. A similar approach to modelling motion interrupted by transient immobilisations was studied in [53]. In the present work we consider a MIM in the formulation with mean mobile residence time τ_m and mean immobile residence time τ_{im} similar to our previous work [54] in the absence of a drift. In [54], the mean immobile residence time τ_{im} and mean mobile residence time τ_m are well separated, $\tau_{\text{im}} \gg \tau_m$, corresponding to the one-dimensional motion of tau proteins without advection. At intermediate times $\tau_m \ll t \ll \tau_{\text{im}}$ a Laplace distribution of positions $\text{const} \times \exp(-\text{const}|x|)/2$ with fixed variance was shown to emerge whose prefactor depends on the initial condition, and the MSD of initially mobile tracers displayed a plateau at intermediate times. The main goal of the present work is to analyse how the Laplace distribution and the plateau in the MSD change when advection is added. The transition from the Brownian MSD $2Dt$ at short times to $2D_{\text{eff}}t$ implies a crossover regime, in which the MSD grows faster than linear given our finding $D_{\text{eff}} > D$. In fact, we find a sustained superdiffusive regime with a cubic anomalous diffusion exponent in the MSD at relevant intermediate time scales. For low advection velocities we recover the model from [54]. Therefore, to highlight new features, we focus on high Péclet numbers $\text{Pe} = v^2\tau_m/(2D) \gg 1$. An application of the MIM with a high Péclet number may occur for sufficiently long times in subsurface aquifers, in the hyperheic zone or in microfluidic setups. A specific example is the motion of biomolecules in bio sensors, as schematically depicted in figure 1. The biomolecules are inserted into a flow cell and bind to the surface reversibly [38]. The surface is coated with receptors that specifically bind to the molecule of interest. Only the bound molecules can be detected using e.g. surface plasmon resonance [38]. In our model we assume the detector to be completely covered with receptors and consider concentrations well below saturation.

In the next section we introduce the model equations and show two ways to solve the model. The direct way using Fourier–Laplace transform yields the densities in Laplace space and exact expressions for the MSD. Additionally, we show how to solve the advection-MIM using a subordination approach, that produces a physical explanation for the additional term in D_{eff} due to the variance of times the tracers spend in the mobile state. As mentioned in the following, we consider strong advection and obtain asymptotic expressions for the density and the MSD in the presence of a clear time scale separation, i.e. $\tau_m \ll \tau_{\text{im}}$ or $\tau_{\text{im}} \ll \tau_m$. For clarity we focus on the detailed behaviour of the MSD of the total density, while the results for the immobile and mobile fractions are summarised in the appendix. The dimensionless form of the model depends on the ratio τ_{im}/τ_m and the Péclet number only. We use these variables in a phase diagram to analyse the anomalous diffusion in the full parameter space including small Péclet numbers. Specifically, in section 2, we formulate and solve our model. In section 3 we consider tracers that are initially mobile and obtain asymptotic

⁵ We use the term ‘residence times’ in the mobile or immobile state to avoid confusion with the waiting times in a continuous time random walk.

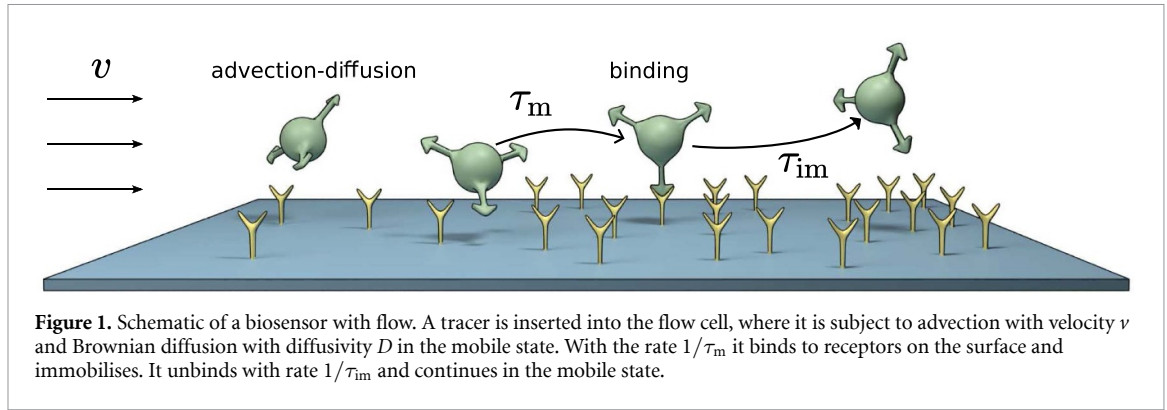


Figure 1. Schematic of a biosensor with flow. A tracer is inserted into the flow cell, where it is subject to advection with velocity v and Brownian diffusion with diffusivity D in the mobile state. With the rate $1/\tau_m$ it binds to receptors on the surface and immobilises. It unbinds with rate $1/\tau_{im}$ and continues in the mobile state.

expressions of the density functions and MSDs. Special focus is put on finding the parameter regimes where non-Gaussian displacement distributions and anomalous scaling of the MSD emerge. In section 4 we repeat the same analysis for initially immobile tracers. Finally, we summarise and conclude in section 5. The appendix provides details on the calculations and additional figures of the MSDs.

2. Formulation of the model

We employ the MIM with mean mobile residence time τ_m and mean immobile residence time τ_{im} in an (effectively) one-dimensional setting with position variable x ,

$$\begin{aligned} \frac{\partial}{\partial t} n_m(x, t) &= -\frac{1}{\tau_m} n_m(x, t) + \frac{1}{\tau_{im}} n_{im}(x, t) - v \frac{\partial}{\partial x} n_m(x, t) + D \frac{\partial^2}{\partial x^2} n_m(x, t) \\ \frac{\partial}{\partial t} n_{im}(x, t) &= -\frac{1}{\tau_{im}} n_{im}(x, t) + \frac{1}{\tau_m} n_m(x, t), \end{aligned} \quad (3)$$

where $n_m(x, t)$ and $n_{im}(x, t)$ denote the line densities of mobile and immobile tracers, respectively. Advection with velocity v and dispersion with diffusion constant D is exclusively affecting the mobile density. A single tracer switches between the mobile state and immobile state following a two state continuous time Markov process, i.e. it follows a Poissonian switching. The realisation (3) of the MIM corresponds to the model used in [54] with the residence time distribution in the mobile state $\gamma(\tau) = \exp(-\tau/\tau_m)/\tau_m$. We add a drift in the mobile state here and will show that this has significant consequences. Splitting the total density $n_{tot}(x, t) = n_m(x, t) + n_{im}(x, t)$ has the advantage that not always $n_{tot}(x, t)$ is measured in experiments. In a biophysics sensor as sketched in [38], solely the immobile tracers can be measured. In contrast, it is often the mobile density that is measured in geological experiments [12, 18]. In both cases it is thus essential to model the two densities separately. Step or delta injection into the mobile domain is common in geological experiments [10, 12, 55–57]. Our model (3) is very similar to the MIMs used in geoscience, with the difference that there usually the capacity coefficients and porosity, among others, are used instead of the mean residence times [6, 7, 13]. We consider the initial condition $n_m(x, 0) = f_m^0 \delta(x)$ and $n_{im}(x, 0) = f_{im}^0 \delta(x)$ where $\delta(x)$ denotes the Dirac- δ distribution. The factors f_m^0 and f_{im}^0 denote the fractions of initially mobile and immobile tracers with $f_m^0 + f_{im}^0 = 1$, which effects the normalisation of the total density, $\int_{-\infty}^{\infty} n_{tot}(x, t) dx = 1$. This corresponds to a single-particle picture with no interactions between the tracers, as is the case in model (3). In this work we consider the cases when all tracers are either initially mobile ($f_m^0 = 1$) or when all tracers are immobile ($f_{im}^0 = 1$). We briefly discuss an equilibrium fraction of initially mobile tracers in appendix K. Other mixed initial conditions are comparatively uninteresting and do not correspond to the experimental initial conditions we have in mind. The structure of this section is as follows. In section 2.1 solutions are derived using Fourier–Laplace transforms. The solution using a subordination approach is shown in section 2.2. In section 2.3 it is demonstrated that the dimensionless formulation of the model (3) model depends on two parameters only. Finally, we discuss the short- and long-time behaviour in sections 2.4 and 2.5.

2.1. Solution in Laplace space

Fourier–Laplace transform $f(k, s) \equiv \int_{-\infty}^{\infty} \int_0^{\infty} f(x, t) \exp(-st + ikx) dt dx$ of the model equations (3) allows solving for the densities, as shown in appendix A. Subsequent Fourier inversion of equations (A.2) and (A.3) produces the expressions

$$n_m(x, s) = \left(f_m^0 + f_{im}^0 \frac{1}{1 + s\tau_{im}} \right) \frac{\exp\left(\frac{vx}{2D}\right)}{\sqrt{v^2 + 4\phi(s)D}} \exp\left(-\sqrt{v^2 + 4\phi(s)D} \frac{|x|}{2D}\right) \quad (4)$$

$$n_{im}(x, s) = \frac{\tau_{im}/\tau_m}{1 + s\tau_{im}} \left(f_m^0 + f_{im}^0 \frac{1}{1 + s\tau_{im}} \right) \frac{\exp\left(\frac{vx}{2D}\right)}{\sqrt{v^2 + 4\phi(s)D}} \exp\left(-\sqrt{v^2 + 4\phi(s)D} \frac{|x|}{2D}\right) + f_{im}^0 \frac{\tau_{im}}{1 + s\tau_{im}} \delta(x) \quad (5)$$

as well as (see equation (A.4))

$$n_{tot}(x, s) = \frac{f_m + f_{im}^0 \frac{1}{1 + s\tau_{im}}}{s} \frac{\phi(s) \exp\left(\frac{vx}{2D}\right)}{\sqrt{v^2 + 4\phi(s)D}} \exp\left(-\sqrt{v^2 + 4\phi(s)D} \frac{|x|}{2D}\right) + f_{im}^0 \frac{\tau_{im}}{1 + s\tau_{im}} \quad (6)$$

with $\phi(s) = s[1 + \tau_{im}\tau_m^{-1}/(1 + s\tau_{im})]$. The fraction $f_m(t) = \int_{-\infty}^{\infty} n_m(x, t)dx$ of free and the fraction $f_{im}(t) = \int_{-\infty}^{\infty} n_{im}(x, t)dx$ of immobile tracers are a function of time and the expressions are given in equation (A.8) in appendix A. From these relations we immediately deduce that the total density is normalised, $f_m(t) + f_{im}(t) = 1$. In the long-time limit, the equilibrium fraction $f_m^{eq} = \tau_m/(\tau_m + \tau_{im})$ of all tracers are mobile. We calculate the p th moment ($p \in \mathbb{N}$) using

$$\langle x^p(t) \rangle_j = \frac{1}{f_j(t)} \int_{-\infty}^{\infty} x^p n_j(x, t) dx, \quad (7)$$

where j stands for m, im, or tot [54]. To shorten the notation, we use $\langle x^2(t) \rangle = \langle x^2(t) \rangle_{tot}$ in the remainder of this work. The lengthy exact expressions for the MSD are given in appendix B. We will study their detailed behaviour below and in sections 3 and 4 for specific initial conditions. The first moment $\langle x(t) \rangle$ is related to the second moment $\langle x^2(t) \rangle_0$ in the advection-free setting with the second Einstein relation [58]

$$\langle x(t) \rangle = \frac{v}{2D} \langle x^2(t) \rangle_0. \quad (8)$$

This relation becomes obvious when we look at the moments in appendix B. Since $\langle x^2(t) \rangle_0$ was discussed in [54] in detail, we focus on the MSD here.

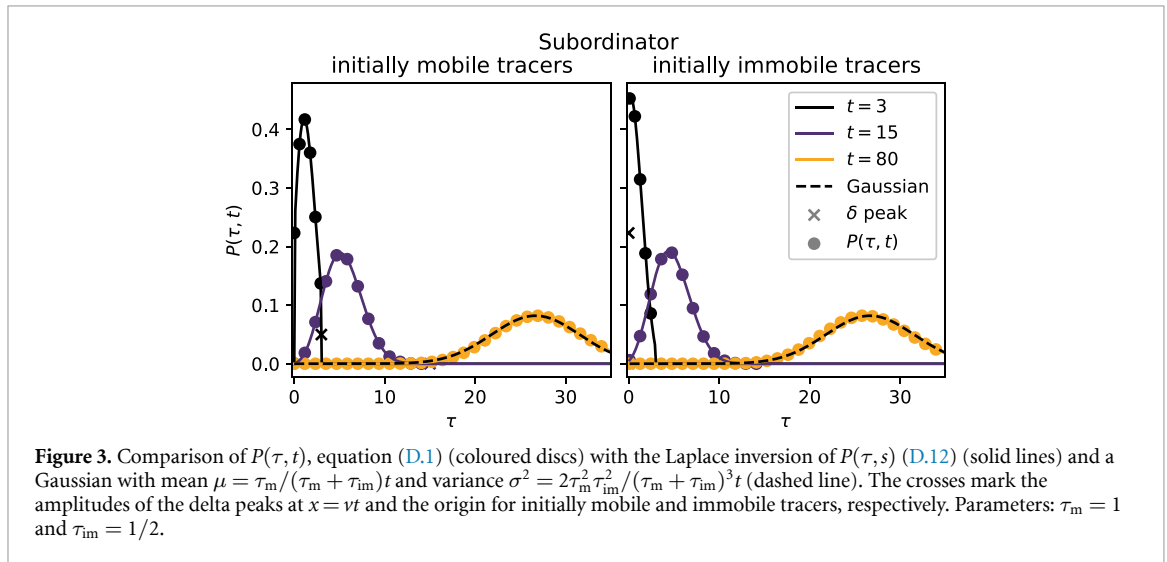
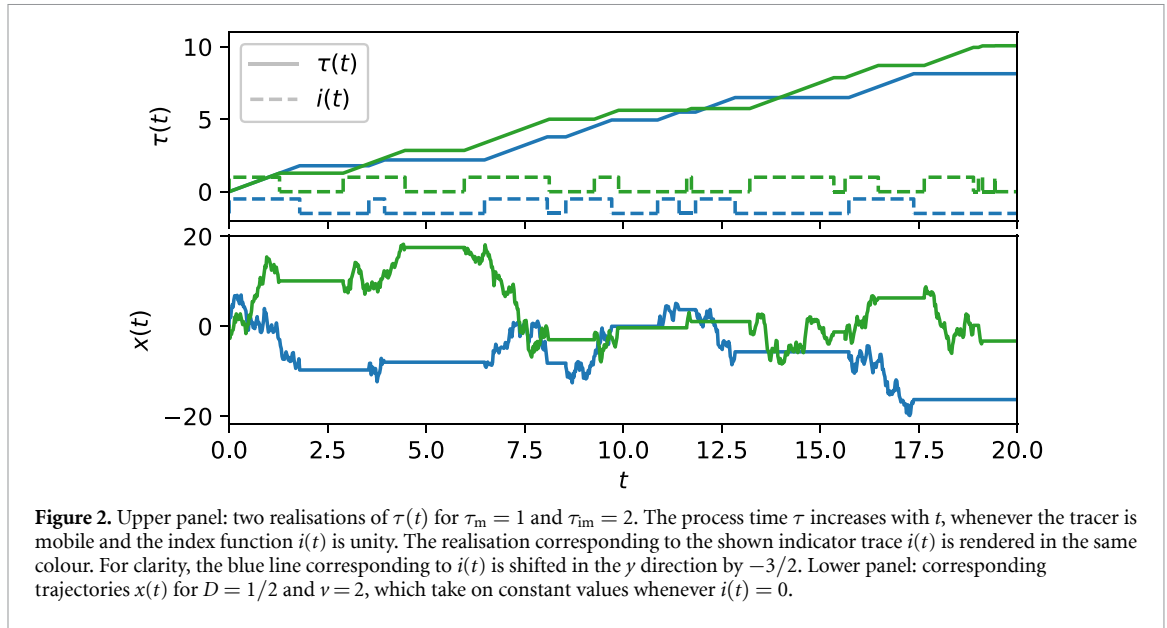
2.2. Subordination approach

The concept of subordination was originally introduced by Bochner [59] and refers to a process $X[\tau(t)]$ with the operational time τ (in many random walk contexts the number of jumps [44]), which has random non-negative increments. For the operational time τ the propagator is known, in our case the Gaussian $G(x, \tau)$ (2). Then, the subordinator relates the stochastic increases of τ to the process (laboratory) time t measured in the real-world observation. In our model the stochasticity comes from the immobilisations, where t increases even while τ is stalling. Assume that we know of a single tracer when it is mobile and when it is immobile. Let $i(t)$ be the index function that is unity if the tracer is mobile at time t and zero otherwise, as shown in figure 2. The index function follows a two-state continuous-time Markov process (telegraph process) with mean residence time τ_m in state 1 and mean residence time τ_{im} in state 0. As described in [60–62] (compare also [63]), this allows us to write a Langevin equation of the form

$$\frac{d}{d\tau} x(\tau) = v + \sqrt{2D}\xi(\tau) \quad (9)$$

$$\frac{d}{dt} \tau(t) = i(t), \quad (10)$$

with the operational time τ , that is a random quantity, and zero-mean white Gaussian noise with correlation $\langle \xi(\tau)\xi(\tau + \Delta\tau) \rangle = \delta(\Delta\tau)$. Figure 2 shows two samples of $\tau(t)$ for $\tau_m = 1$ and $\tau_{im} = 2$ in the upper panel. The lower panel shows the corresponding trajectory $x(t)$ for $D = 1/2$ and $v = 2$. The propagator with this new variable τ is given by $G(x, \tau)$ (2). In appendix D we show how to obtain the subordinator $P(\tau, t)$ and its moments using Laplace transforms. In figure 3 we show the numerical Laplace inversion of $P(\tau, s)$ (D.12) for three values of t and the parameters $\tau_m = 1$ and $\tau_{im} = 1/2$. In order to verify our approach, we compare the Laplace inversion to the solution $P(\tau, t)$ obtained in [23], that is presented in appendix D. We find good agreement between the two approaches, as shown in figure 3. In the long-time limit $P(\tau, t)$ converges to a Gaussian with mean $\mu = t\tau_m/(\tau_m + \tau_{im})$ and variance $\sigma^2 = 2\tau_m^2\tau_{im}^2/(\tau_m + \tau_{im})^3 t$, as shown by the dashed



line following a Gaussian with that mean and variance (see the moments above). With $P(\tau, t)$ we can eliminate $\tau(t)$ and find using the well established method of subordination [60–65]

$$n_{\text{tot}}(x, t) = \int_0^\infty P(\tau, t) G(x, \tau) d\tau, \quad (11)$$

where $G(x, t)$ denotes the propagator (18) in the mobile phase. Expression (11) can be written in the form (6) of $n_{\text{tot}}(x, s)$ by inserting the subordinator $P(\tau, s)$ in Laplace space. In appendix D we show how to obtain $n_m(x, t)$ and $n_{im}(x, t)$ in a similar way.

2.3. Dimensionless form

Our model (3) has the four parameters τ_m , τ_{im} , ν and D . We now show that in a dimensionless form the model depends only on two free parameters, which significantly reduces the space of parameters we need to consider in order to obtain a full picture of the model. Moreover, this highlights the conceptual simplicity of the model. To this end, we define the new dimensionless variables $t' = t/\tau_m$ and $x' = x/\sqrt{D\tau_m}$. In these variables the model (3) turns into the set of equations

$$\begin{aligned} \frac{\partial}{\partial t'} n_m(x', t') &= -n_m(x', t') + \frac{\tau_m}{\tau_{im}} n_{im}(x', t') \\ &\quad - \sqrt{2\text{Pe}} \frac{\partial}{\partial x'} n_m(x', t') + \frac{\partial^2}{\partial x'^2} n_m(x', t') \end{aligned} \quad (12)$$

$$\frac{\partial}{\partial t'} n_{\text{im}}(x', t') = -\frac{\tau_{\text{m}}}{\tau_{\text{im}}} n_{\text{im}}(x', t') + n_{\text{m}}(x', t'), \quad (13)$$

which only depends on the immobilisation ratio $\tau_{\text{im}}/\tau_{\text{m}}$ and the Péclet number $\text{Pe} = v^2\tau_{\text{m}}/(2D)$. The typical length scale for the latter is given by $v\tau_{\text{m}}$. The factor $1/2$ in the Péclet number is introduced for convenience. To see this, we note that from the Péclet number we obtain the advection time scale $\tau_{\text{v}} = 2D/v^2$, which naturally arises from the solution to the advection-diffusion equation (2) as follows. The typical distance travelled due to advection and dispersion is given by $\Delta x_{\text{v}} = vt$ and $\Delta x_{\text{D}} = \sqrt{2Dt}$, respectively. Comparing these distances gives the time scale $\tau_{\text{v}} = 2D/v^2 = \tau_{\text{m}}/\text{Pe}$, after which displacements due to advection dominate over diffusive displacements.

2.4. Short-time behaviour

In the mobile phase tracers are being propagated with the Gaussian (2). As described above the displacements are diffusion dominated for $t \ll \tau_{\text{v}}$. This means that the tracers follow the same density as in the case without advection, which is described in detail in [54]. To emphasise the effects of advection we therefore choose $\tau_{\text{v}} \ll \tau_{\text{m}}, \tau_{\text{im}}$. This defines the short-time limit $t \ll \tau_{\text{v}}$.

2.5. Long-time asymptote

The densities of the total, mobile and immobile density are, up to a factor, the same in the long-time limit $t \gg \tau_{\text{m}}, \tau_{\text{im}}$ [5]. In absence of advection, the effective long-time diffusivity is given by $D_{\text{eff}} = D\tau_{\text{m}}/(\tau_{\text{m}} + \tau_{\text{im}})$ for $t \gg \tau_{\text{m}}, \tau_{\text{im}}$ [54]. Tracers disperse slower compared to the model of simple diffusion advection without immobilisation (1) with diffusivity D . We now obtain D_{eff} by analysing the asymptotic behaviour $t \gg \tau_{\text{m}}, \tau_{\text{im}}$ of the expressions for the MSD. The exact expressions for the first and second moments are stated in appendix B. These results provide the long-time asymptote of the MSD for all initial conditions, namely,

$$\langle [x(t) - \langle x(t) \rangle]^2 \rangle \sim 2 \left(D \frac{\tau_{\text{m}}}{\tau_{\text{m}} + \tau_{\text{im}}} + \frac{v^2 \tau_{\text{m}}^2 \tau_{\text{im}}^2}{(\tau_{\text{m}} + \tau_{\text{im}})^3} \right) t, \text{ for } t \gg \tau_{\text{m}}, \tau_{\text{im}}, \quad (14)$$

where \sim denotes asymptotic equivalence with an additional spread $\propto v^2 t$ compared to the case without advection. Remarkably, the asymptotic dispersion with the new effective diffusion coefficient

$$D_{\text{eff}} = D \frac{\tau_{\text{m}}}{\tau_{\text{m}} + \tau_{\text{im}}} + v^2 \frac{\tau_{\text{m}}^2 \tau_{\text{im}}^2}{(\tau_{\text{m}} + \tau_{\text{im}})^3} \quad (15)$$

can hence even be higher than the diffusivity D in the mobile state and overcompensate the slow-down of the spread due to immobile durations. In appendix H we explore the parameter regime that yields $D_{\text{eff}} > D$. As shown in figure H1, the increase of D_{eff} is highest, when τ_{m} and τ_{im} are of the same order. A physical intuition for the additional spread due to advection arises from the special case $D = 0$, for which $x = v\tau$ with the mobile duration τ . Due to the stochastic switching between the mobile and immobile state, an ensemble of tracers will have a distribution of mobile durations τ (the density $P(\tau, t)$ in section 2.2), and hence the positions will have a finite spread. This additional spread was derived before [6, 13], albeit without a more detailed physical justification. The anomalous transport regime at intermediate times that necessarily has to exist to effect the crossover between the two normal-diffusive regimes, and the important physical consequences will not be explained⁶. We explore the physical mechanism behind the additional dispersion due to advection in the long-time asymptote (14) of the MSD. We start by discretising the advection-diffusion process into discrete steps Δx_i that are normally distributed $\Delta x_i \stackrel{\text{d}}{=} \mathcal{N}(v\Delta t, 2D\Delta t)$, where each step takes a small duration $\Delta t \ll t, \tau_{\text{m}}, \tau_{\text{im}}$. After n steps the tracer position is given by $\sum_{i=1}^n \Delta x_i = x$. In the long-time limit the number of steps n follows a Gaussian $n \stackrel{\text{d}}{=} \mathcal{N}(\mu/\Delta t, \sigma^2/(\Delta t)^2)$, as described in section 2.2⁷. The number of steps n is independent of the steps Δx_i . With the expectation value \mathbb{E} and the variance var we obtain the expression [66]

$$\text{var}(x) = \mathbb{E}(n)\text{var}(\Delta x_i) + (\mathbb{E}(\Delta x_i))^2 \text{var}(n) \sim 2 \left(D \frac{\tau_{\text{m}}}{\tau_{\text{m}} + \tau_{\text{im}}} + \frac{v^2 \tau_{\text{m}}^2 \tau_{\text{im}}^2}{(\tau_{\text{m}} + \tau_{\text{im}})^3} \right) t, \quad (16)$$

⁶ Later we will demonstrate that the transient anomalous diffusion regime can assume substantial time spans with an approximately constant anomalous diffusion exponent.

⁷ The Gaussian distribution $n \stackrel{\text{d}}{=} \mathcal{N}(\mu/\Delta t, \sigma^2/(\Delta t)^2)$, that only applies in the long-time limit, in principle allows for negative numbers of steps. However, they asymptotically vanish, because the width of the distribution vanishes compared to the mean. We quantify this using the coefficient of variation of step numbers $\sqrt{\text{var}(n)}/\mathbb{E}(n) \sim \tau_{\text{im}}(\tau_{\text{m}} + \tau_{\text{im}})^{-1/2} t^{-1/2} \rightarrow 0$ for $t \gg \tau_{\text{m}}, \tau_{\text{im}}$. Note that here $\stackrel{\text{d}}{=}$ means equivalence in distribution.

for $t \gg \tau_m, \tau_{im}$. Equation (16) demonstrates that in the case of diffusion without advection only the mean mobile duration affects the MSD. In contrast, advection couples to the mean in the first moment and to the variance of the duration that the tracers spend in the mobile state in the MSD (14).

All time scales in the model are finite, and therefore the density converges to the Gaussian

$$n_{tot}(x, t) \sim \frac{1}{\sqrt{4\pi D_{eff}t}} \exp\left(-\frac{(x - v_{eff}t)^2}{4D_{eff}t}\right) \quad \text{for } t \gg \tau_m, \tau_{im} \quad (17)$$

in the long-time limit with the effective diffusion coefficient D_{eff} (equation (15)) and the effective advection velocity $v_{eff} = v\tau_m/(\tau_m + \tau_{im})$ (see appendix B.1). In the next two sections we analyse the densities and MSDs for the specific choice of initially mobile and immobile tracers, respectively.

3. Initially mobile tracers

In this section we assume all tracers to be initially mobile. This situation corresponds to many experimental realisations, when tracers are introduced into the system, such that they have not had a chance to immobilise. We consider the following four aspects. In section 3.1 we assume $\tau_v \ll \tau_m \ll \tau_{im}$, which corresponds to a high Péclet number and long immobilisations to emphasise the effect of advection compared to [54]. In section 3.2 we consider the density for short immobilisations and high Péclet numbers, $\tau_v \ll \tau_{im} \ll \tau_m$. The third section 3.3 is concerned with the MSD for which we obtain expressions for superdiffusion at intermediate time scales arising due to advection. In the final subsection appendix I.1 we analyse for which parameters the uncovered superdiffusive regime exists and how it is competing with the plateau regime in the MSD found in [54] for long immobilisations in the advection-free regime.

3.1. Densities for long immobilisations

Initially mobile tracers that have not yet immobilised follow a Gaussian distribution corresponding to free Brownian motion without advection for $t \ll \tau_m$. At short times $t \ll \tau_v$ advection is negligible in the Gaussian propagator and the density is the same Gaussian with mean $vt \ll \sqrt{2Dt}$ close to zero and variance $2Dt$. At intermediate times $\tau_v \ll t \ll \tau_m$ advection becomes relevant, and the mobile density takes on the Gaussian form

$$n_m(x, t) \sim \left(1 - \frac{t}{\tau_m}\right) \frac{\exp\left(-\frac{(x-vt)^2}{4Dt}\right)}{\sqrt{4\pi Dt}} \quad (18)$$

with $\int_{-\infty}^{\infty} n_m(x, t) dx \sim 1 - t/\tau_m$ corresponding to a scaled solution of the simple diffusion advection equation (1)⁸. The Gaussian (18) is shown as a dashed red line in the first two panels of figure 4, in which a stacked position histogram from simulations is shown in which the colours denote the number of immobilisation events N_{im} . The solid lines are obtained from Laplace inversion of $n_m(x, s)$, $n_{im}(x, s)$, and $n_{tot}(x, s)$ from equations (5) and (6). We use the parameters $\tau_m = 1$, $\tau_{im} = 100$, $D = 1/2$ and $v = 100$. These parameters are specifically chosen to be able to resolve the multiple time regimes. In the short to intermediate time regime $t \ll \tau_m, \tau_{im}$, where t can be shorter or longer than τ_v , the immobile density consists of tracers that immobilised at most once. In equation (F.2) in appendix F we arrive at the asymptotic expression

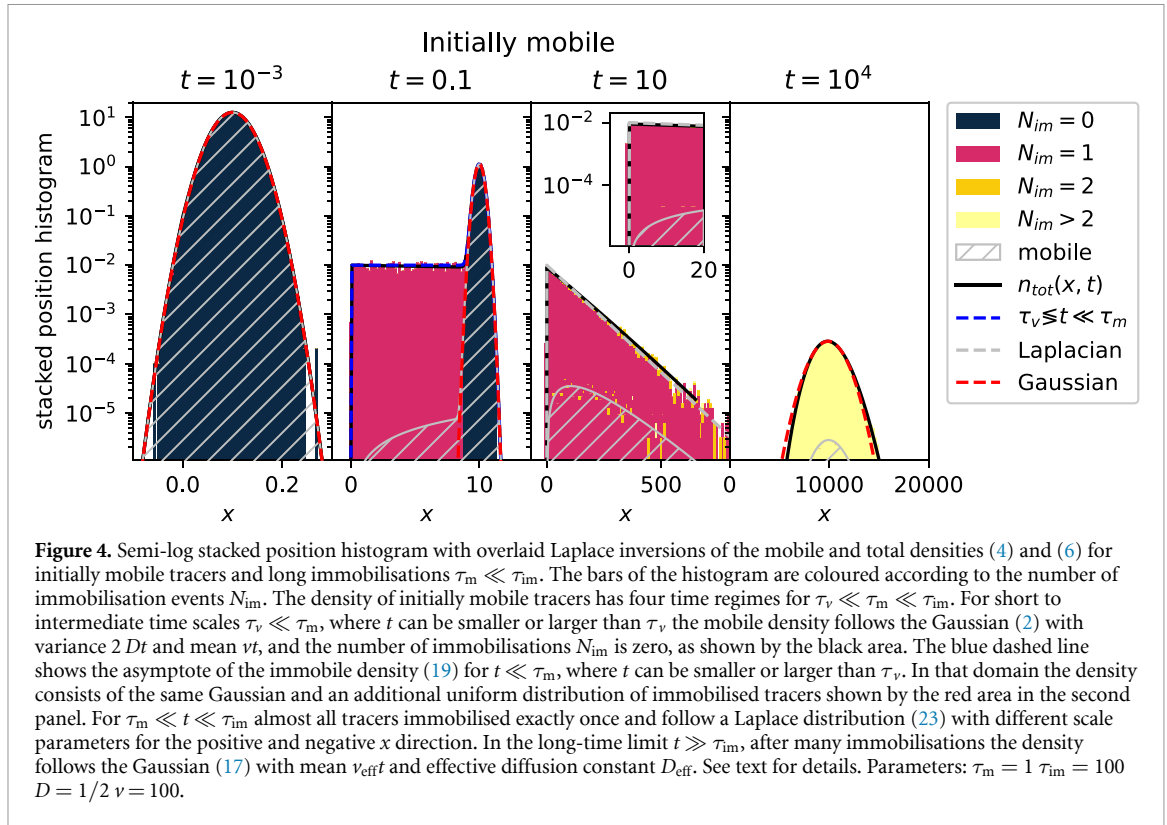
$$n_{im}(x, t) \sim \left[1 + \operatorname{erf}\left(\frac{vt - |x|}{\sqrt{4Dt}}\right) + \exp\left(\frac{v|x|}{D}\right) \left(\operatorname{erf}\left(\frac{vt + |x|}{\sqrt{4Dt}}\right) - 1\right)\right] \times \frac{\exp\left(\frac{vx - v|x|}{2D}\right)}{2v\tau_m} \quad (19)$$

for $t \ll \tau_m, \tau_{im}$. The mass corresponding to (19) is $\int_{-\infty}^{\infty} n_{im}(x, t) dx \sim t/\tau_m$, corresponding to 10^{-3} in the left panel of figure 4. This value is very small and hence the immobile density is not visible in the first panel.

The immobile density in figure 4 appears to be uniform at $t = 0.1$. Indeed, for $\tau_v \ll t$ the short-time density (19) approaches a uniform distribution. Using the properties of the error function we arrive at the asymptotic uniform distribution

$$n_{im}(x, t) \sim \begin{cases} \frac{1}{\tau_m v} & \text{for } 0 < x < vt \\ 0 & \text{otherwise} \end{cases}, \quad (20)$$

⁸ Equation (18) can be obtained by solving equation (3) for $\tau_{im} \rightarrow \infty$.



valid for $\tau_v \ll t \ll \tau_m, \tau_{im}$. This shape can indeed be seen in the second panel of figure 4, for which the immobile density remains almost constant for $0 < x < 10$. The approximation (19) is shown as the blue dashed line. In the same panel the Gaussian (18) is shown as the dashed red line. The total density is given by

$$n_{tot}(x, t) \sim \left(1 - \frac{t}{\tau_m}\right) \frac{\exp\left(-\frac{(x-vt)^2}{4Dt}\right)}{\sqrt{4\pi Dt}} + \begin{cases} \frac{1}{\tau_m v} & \text{for } 0 < x < vt \\ 0 & \text{otherwise} \end{cases} \quad (21)$$

for $\tau_v \ll t \ll \tau_m, \tau_{im}$ with $\int_{-\infty}^{\infty} n_{tot}(x, t) dx = 1$. The appearance of this regime is new, as compared to the case without advection [54]. A physical picture for the occurrence of the uniform density of immobile tracers is as follows. For $\tau_v \ll t \ll \tau_m$ advective transport dominates over diffusion. Indeed, the typical distance a tracer moved due to advection is given by the mean position vt , while the typical distance travelled due to diffusion is given by the standard deviation $\sqrt{2Dt}$. The mobile tracers hence move with a narrow Gaussian distribution while a fraction of tracers immobilises with the constant rate $1/\tau_m$, which generates the uniform part of the distribution (see figure 4 for $t = 0.1$).

Now we go to immobilisation dominated intermediate times $\tau_m \ll t \ll \tau_{im}$. This regime is easy to analyse when starting from the density in Laplace space. We have $\phi(s) \sim 1/\tau_m$ for $s\tau_m \ll 1 \ll s\tau_{im}$ and find the expression

$$n_{tot}(x, s) \sim \frac{1}{s} \frac{\exp\left(\frac{vx}{2D}\right)}{\sqrt{v^2\tau_m^2 + 4D\tau_m}} \exp\left(-\sqrt{v^2 + 4D/\tau_m} \frac{|x|}{2D}\right) \quad (22)$$

from $n_{tot}(x, s)$ (6), which in time-domain corresponds to

$$n_{tot}(x, t) \sim \frac{\exp\left(\frac{vx}{2D}\right)}{\sqrt{v^2\tau_m^2 + 4D\tau_m}} \exp\left(-\sqrt{v^2\tau_m^2 + 4D\tau_m} \frac{|x|}{2D\tau_m}\right), \quad (23)$$

for $\tau_m \ll t \ll \tau_{im}$. Expression (23) is a normalised distribution with time-independent parameters, that falls off exponentially in the positive and negative x direction with different coefficients. It is shown in the third panel in figure 4 for $t = 10$ as the grey dashed line. The density falls off quicker in the direction opposite to the advection velocity, as expected. Noteworthy, the Laplace distribution occurs for all values of the Péclet number, i.e. v can take on any value in the asymptote (23).

For long times $t \gg \tau_{\text{im}}$, we show the Gaussian (17) in figure 4 as a red dashed line for $t = 10^4$. The Gaussian (17) contains the effective advection $v_{\text{eff}} = v\tau_m/(\tau_m + \tau_{\text{im}})$ and the effective diffusivity (15), that we obtained in section 2.5.

3.2. Densities for short immobilisations

Now we turn to the case of short mean immobile residence times, $\tau_{\text{im}} \ll \tau_m$. For short times $t \ll \tau_v$ and intermediate times $\tau_v \ll t \ll \tau_{\text{im}} \ll \tau_m$ the mobile density follows the same Gaussian (18) as for long immobilisations. This can be seen in figure 5 in the first panel for $t = 0.1$. From simulations, we obtain position histograms that we colour-code according to the number of immobilisations. Most tracers have not immobilised at this time, as shown by the dominant black area that follows the Gaussian (18). The tracers that did immobilise follow the same asymptote (19) of $n_{\text{im}}(x, t)$ as for long immobilisations, as depicted by the dashed blue line. Beyond τ_{im} immobile tracers become mobile again and contribute to the mobile density. This can be seen in figure 5 in the second panel for $t = 1$ by the red area in the mobile density denoting tracers with a single immobilisation event. In figure 5, the total density appears to have an exponential tail in the opposite direction of the advection velocity for $t = 10$ and $t = 20$ in the third and fourth panel, respectively. We now investigate the origin of this phenomenon. For $t \ll \tau_m$, the fraction t/τ_m of mobile tracers is trapped for a short period τ drawn from $\gamma(\tau) = \exp(-\tau/\tau_{\text{im}})/\tau_{\text{im}}$. This is shown as the red area in figure 5 denoting a single immobilisation. Hence, these tracers were mobile for a total period of $t - \tau$. We convolute this with the propagator for advection diffusion. Together with tracers that have not immobilised this gives the total density for $\tau_m \ll t \ll \tau_{\text{im}}$,

$$n_{\text{tot}}(x, t) \sim \left(1 - \frac{t}{\tau_m}\right) \frac{\exp\left(-\frac{(x-vt')^2}{4Dt'}\right)}{\tau_m \sqrt{4\pi Dt'}} + \frac{t}{\tau_m} \int_0^t \frac{\exp\left(-\frac{(x-vt')^2}{4Dt'}\right)}{\tau_{\text{im}} \sqrt{4\pi Dt'}} e^{-(t-t')/\tau_{\text{im}}} dt'. \quad (24)$$

The integral on the right-hand side can be solved and is given by

$$\int_0^t \frac{\exp\left(-\frac{(x-vt')^2}{4Dt'}\right)}{\tau_{\text{im}} \sqrt{4\pi Dt'}} e^{-(t-t')/\tau_{\text{im}}} dt' \sim \frac{\exp\left(-\frac{t}{\tau_{\text{im}}}\right)}{2v\tau_{\text{im}}} \left[\exp\left(\frac{x}{v\tau_{\text{im}}}\right) \text{erfc}\left(\frac{x-tv}{2\sqrt{Dt}}\right) - \exp\left(\frac{vx}{D}\right) \text{erfc}\left(\frac{x+vt}{2\sqrt{Dt}}\right) \right], \quad (25)$$

for $v^2\tau_{\text{im}} \gg D$ with the complimentary error function $\text{erfc}(x) = 1 - \text{erf}(x)$. In appendix G we develop the full expression of the integral (25), that is also valid for $v^2\tau_{\text{im}} \sim D$, i.e. intermediate Péclet numbers.

Approximation (24) is shown in figure 5 as the dashed dark-yellow line and follows the density for $x > 70$ at $t = 10$ and matches almost the entire density at $t = 20$. For $x \ll vt$ and $v^2\tau_{\text{im}} \gg D$ expression (24) simplifies to

$$n_{\text{tot}}(x, t) \sim \frac{t}{\tau_m} \frac{\exp\left(-\frac{t}{\tau_{\text{im}}} + \frac{x}{v\tau_{\text{im}}}\right)}{v\tau_{\text{im}}}, \quad \text{for } \tau_{\text{im}} \ll t \ll \tau_m \text{ and } 0 < x \ll vt. \quad (26)$$

This tail approximation is only valid close the origin. For this reason it is not normalised. It is shown in figure 5 as the solid grey line. The tail overlaps with expression (24) shown as the dashed dark-yellow line. The second exponent in expression (26) reveals that the slope of the tail does not depend on time. The slope decreases for larger values of τ_{im} . As described in detail in section 2.5 the long-time asymptote $t \gg \tau_m$ of the density follows a Gaussian with an effective advection speed and an effective diffusivity.

3.3. Mean squared displacement

In this section we analyse the MSD of the total density. In appendices E.1.1 and E.1.2 we analyse the MSD of the immobile and mobile density, respectively. We now investigate how advection changes the MSD as compared to the results presented in [54]. Table C1 shows a series of the total, mobile and immobile MSDs for initially mobile and initially immobile tracers for $t \ll \tau_m, \tau_{\text{im}}$. In all cases, the leading order term does not depend on v . Therefore, for short times the MSDs are equivalent to the MSD without advection.

In figure 6(a) the MSD for initially mobile tracers is shown for long immobilisations, $\tau_m \ll \tau_{\text{im}}$, where the solid black line corresponds to the total density's MSD. In panel (b) we show the MSDs for short immobilisations, $\tau_{\text{im}} \ll \tau_m$. For comparison, we show the MSD for the case without advection in grey. It can be seen that the corresponding MSDs with and without advection overlap for $t \ll \tau_v$. After a linear

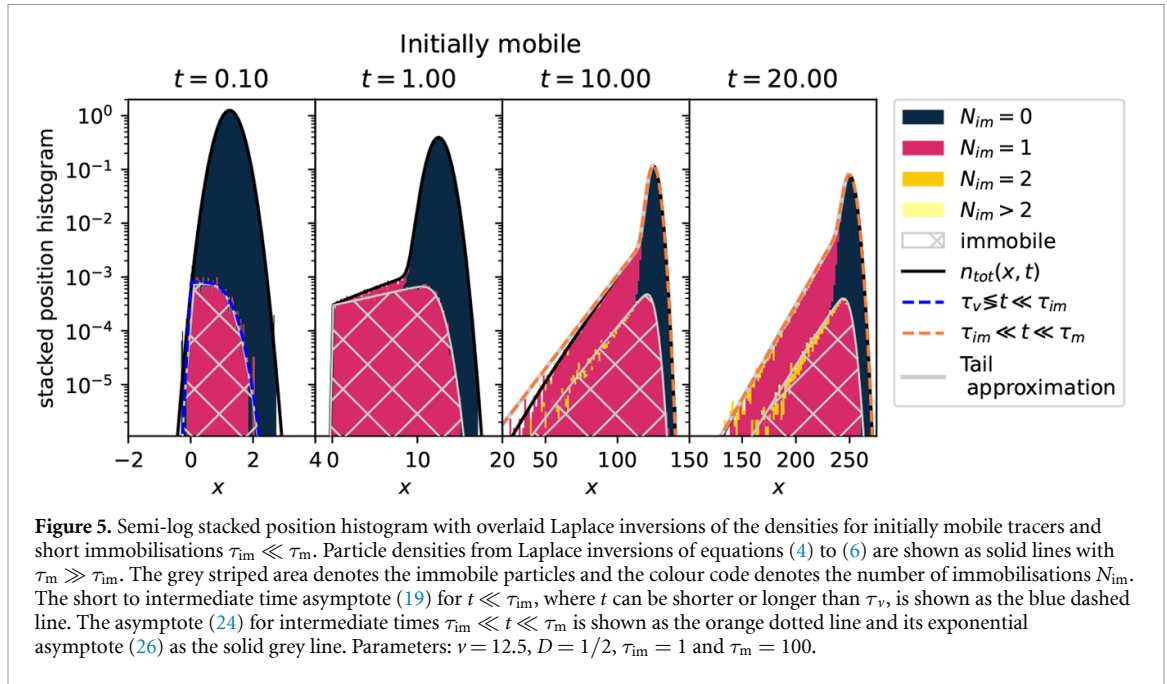


Figure 5. Semi-log stacked position histogram with overlaid Laplace inversions of the densities for initially mobile tracers and short immobilisations $\tau_{im} \ll \tau_m$. Particle densities from Laplace inversions of equations (4) to (6) are shown as solid lines with $\tau_m \gg \tau_{im}$. The grey striped area denotes the immobile particles and the colour code denotes the number of immobilisations N_{im} . The short to intermediate time asymptote (19) for $t \ll \tau_{im}$, where t can be shorter or longer than τ_v , is shown as the blue dashed line. The asymptote (24) for intermediate times $\tau_{im} \ll t \ll \tau_m$ is shown as the orange dotted line and its exponential asymptote (26) as the solid grey line. Parameters: $v = 12.5$, $D = 1/2$, $\tau_{im} = 1$ and $\tau_m = 100$.

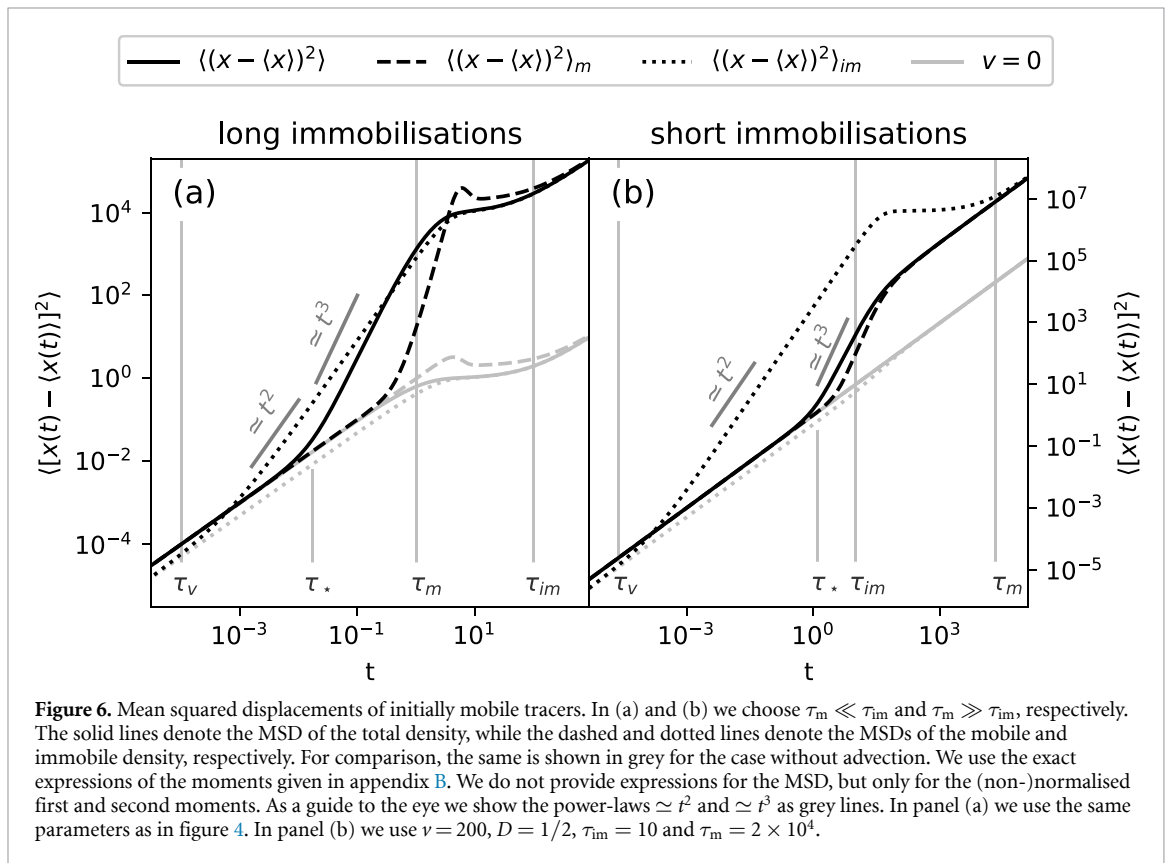


Figure 6. Mean squared displacements of initially mobile tracers. In (a) and (b) we choose $\tau_m \ll \tau_{im}$ and $\tau_m \gg \tau_{im}$, respectively. The solid lines denote the MSD of the total density, while the dashed and dotted lines denote the MSDs of the mobile and immobile density, respectively. For comparison, the same is shown in grey for the case without advection. We use the exact expressions of the moments given in appendix B. We do not provide expressions for the MSD, but only for the (non-)normalised first and second moments. As a guide to the eye we show the power-laws $\simeq t^2$ and $\simeq t^3$ as grey lines. In panel (a) we use the same parameters as in figure 4. In panel (b) we use $v = 200$, $D = 1/2$, $\tau_{im} = 10$ and $\tau_m = 2 \times 10^4$.

short-time behaviour for $t \ll \tau_*$ the MSD crosses over to a cubic scaling for $\tau_* \ll t \ll \tau_m, \tau_{im}$. Our goal is to quantify the cubic scaling and determine the value of τ_* . From a series expansion of the exact expression for the MSD (exact expressions for the moments are given in appendix B), we obtain the asymptotic MSD

$$([x(t) - \langle x(t) \rangle]^2) \sim 2Dt + \frac{v^2}{3\tau_m} t^3, \text{ for } t \ll \tau_m, \tau_{im}. \quad (27)$$

In figure E2 we compare equation (27) to the full expression of the MSD and find very nice agreement. A cubic scaling of the MSD (27) emerges at intermediate times when the cubic term dominates over the linear term in equation (27). This corresponds to the relation $\tau_* \ll t \ll \tau_m$ with $\tau_* = \sqrt{3\tau_v\tau_m}$. Indeed, the cubic

scaling of the total MSD is shown in figure 6(a) in the domain $\tau_* \ll t \ll \tau_m$. Notably, it occurs also for $\tau_{im} \ll \tau_m$, as shown in figure 6(b). This cubic scaling is new compared to the case without advection. It lies within the domain where we found an advection dominated regime $\tau_v \ll t \ll \tau_m$ in the previous section, in which the density (21) consists of a uniform and a Gaussian distribution with time-dependent weights. In figure E1 we show the MSD and choose such parameters that emphasise that the intermediate cubic scaling can be more than a bare crossover but corresponds to a distinct anomalous regime. We now show that the anomalous diffusion arises from this distribution. First we consider the uniform distribution ranging from zero to vt . It has the first moment $\langle x(t) \rangle_{im} = \frac{vt}{2}$ and the second moment $\langle x(t)^2 \rangle = \frac{v^2 t^2}{3}$ with the MSD $\langle (x(t) - \langle x(t) \rangle)^2 \rangle_{im} = \frac{v^2 t^2}{12}$. This is the dominating term of the immobile density's MSD for $\tau_v \ll t \ll \tau_m, \tau_{im}$, as shown in figures 6(a) and (b), where the quadratic scaling can be observed. Second we recall the first and second moments of the mobile Gaussian distribution $\langle x(t) \rangle_m = vt$ and $\langle x(t)^2 \rangle = v^2 t^2 + 2Dt$. Now we consider the MSD of the total density by combining the moments with the normalisations t/τ_m and $1 - t/\tau_m$ for the uniform and Gaussian distribution, respectively. This leads to the same asymptotic MSD (27), as obtained by the series expansion, as the following calculation shows:

$$\begin{aligned} \langle x(t) \rangle &= \langle x(t) \rangle_{im} \frac{t}{\tau_m} + \langle x(t) \rangle_m \left(1 - \frac{t}{\tau_m}\right) = vt - \frac{vt^2}{2\tau_m} \\ \langle x(t)^2 \rangle &= \langle x(t)^2 \rangle_{im} \frac{t}{\tau_m} + \langle x(t)^2 \rangle_m \left(1 - \frac{t}{\tau_m}\right) = -\frac{2}{3} \frac{v^2 t^3}{\tau_m} + v^2 t^2 - 2D \frac{t^2}{\tau_m} + 2Dt \\ \langle [x(t) - \langle x(t) \rangle]^2 \rangle &= 2Dt - 2D \frac{t^2}{\tau_m} + \frac{v^2 t^3}{3\tau_m} - \frac{v^2 t^4}{4\tau_m^2} \\ &\sim 2Dt + \frac{v^2}{3\tau_m} t^3, \text{ for } t \ll \tau_m \ll \tau_{im}. \end{aligned} \quad (28)$$

The asymptotic expression is identical to what we found from the exact expressions (27). This shows indeed that the uniform distribution and the Gaussian distribution can indeed explain the cubic scaling. The cubic scaling of the MSD emerges for $\tau_* \ll t \ll \tau_m, \tau_{im}$. This means that for long immobilisations $\tau_m \ll \tau_{im}$ the advection needs to be sufficiently large such that $\tau_v = 2D/v^2 \ll \tau_m$, as shown in figure 6(a). The cubic scaling emerges for short immobilisations $\tau_{im} \ll \tau_m$, as well. In that case the Péclet number needs to satisfy $Pe \gg 3\tau_m^2/\tau_{im}^2$. In appendix I we discuss the parameter regimes for which cubic scaling emerges in detail.

Now we choose long immobilisations, $\tau_{im} \gg \tau_m$, and consider the intermediate immobilisation dominated regime $\tau_m \ll t \ll \tau_{im}$. In the absence of advection we found a plateau of the total MSD shown as the grey solid line in figure 6(a). Compared to [54] we here choose a high Péclet number, $v^2 \tau_m/2D \gg 1$, and keep the time scale separation $\tau_m \ll \tau_{im}$ here. The plateau still exists at $\tau_m \ll t \ll \tau_{im}$, although at a higher value as shown by the black solid line in figure 6(a). The existence of the plateau comes as no surprise, because the physical mechanism of the plateau remains unchanged. All tracers are initially mobile and have immobilised for $\tau_m \ll t \ll \tau_{im}$, as shown in figure 4 for $t = 10$. When all tracers are immobile the density does not change and hence the MSD remains constant. Analytically, this can be seen most easily from the expressions of the moments in Laplace space

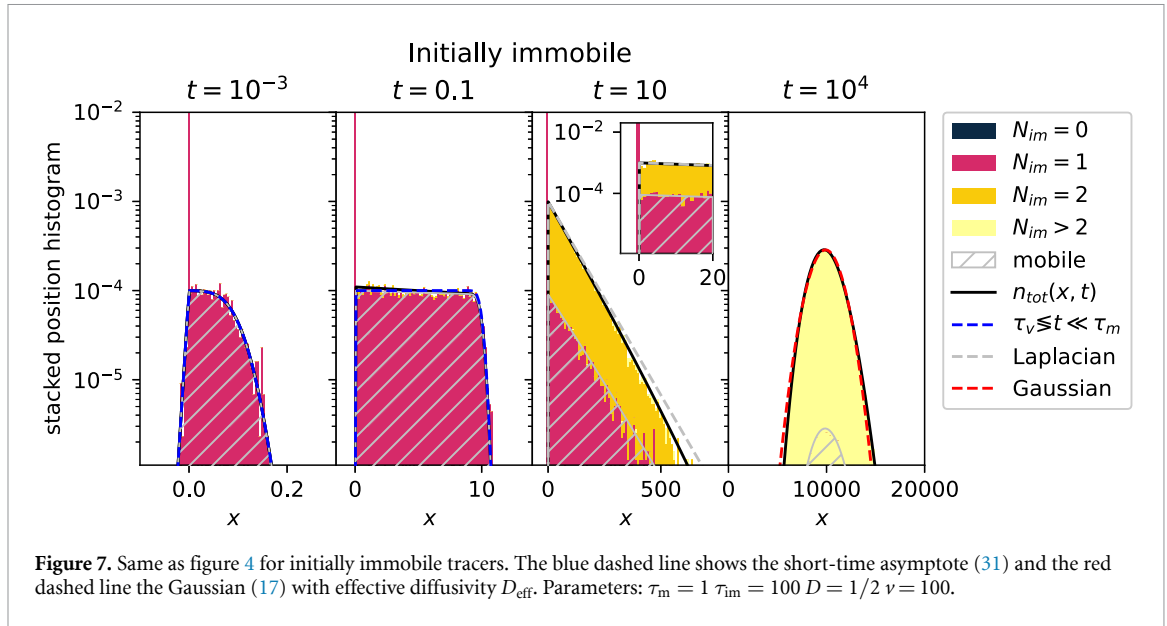
$$\langle x(s) \rangle = \frac{v}{s\phi(s)} \quad (29)$$

$$\langle x^2(s) \rangle = \frac{2v^2}{s\phi^2(s)} + \frac{2D}{s\phi(s)}, \quad (30)$$

that we obtain from expression (A.5). For $\tau_m \ll t \ll \tau_{im}$, we have $\phi(s) \sim 1/\tau_m$, which is a constant. Since the Laplace inverse $\mathcal{L}^{-1}[1/s] = 1$ we obtain a constant MSD in this time-domain $\tau_m \ll t \ll \tau_{im}$, where we observe the asymmetric Laplace distribution (23). We emphasise that the plateau exists regardless of the values of v and D . At long times $t \gg \tau_m, \tau_{im}, \tau_v$ the MSD grows linearly with the effective diffusion coefficient $D_{\text{eff}} = D \frac{\tau_m}{\tau_m + \tau_{im}} + v^2 \frac{\tau_m^2 \tau_{im}}{(\tau_m + \tau_{im})^2}$, as described in section 2.5.

4. Initially immobile tracers

In this section we consider initially immobile tracers. Experimentally, this may correspond to the situation when tracers are released into a microfluidic setup and (part of them) allowed to bind to the sensor receptors. Subsequently, the mobile tracers are flushed out, and then the recording is started. In section 4.1 we report the density for long immobilisations, $\tau_m \ll \tau_{im}$, and high Péclet numbers. In section 4.2 we repeat the same steps for short immobilisations, $\tau_{im} \ll \tau_m$. Section 4.3 is concerned with the MSD, and in the



fourth subsection appendix J.1 we analyse for which parameters a cubic scaling of the MSD emerges at intermediate time scales.

4.1. Density for long immobilisations

We assume long immobilisations, $\tau_m \ll \tau_{im}$, corresponding to the case studied in [54]. We choose a high Péclet number to emphasise the effect of advection, in contrast to the $v = 0$ case in [54]. At short times $t \ll \tau_v$ the propagator for mobile tracers is the same Gaussian as for the case $v = 0$. Therefore, we obtain the same short-time densities as in the $v = 0$ case, i.e. a δ -peak at the origin and an additional non-Gaussian distribution.

At short to intermediate times, $t \ll \tau_m, \tau_{im}$, at which t can be shorter or longer than τ_v , most initially immobile tracers are concentrated at the origin and only gradually mobilise. This gives rise to the immobile density $n_{im}(x, t) \sim (1 - t/\tau_{im})\delta(x)$. As described in detail in [54], immobile tracers that were initially mobile follow the same density as mobile tracers that were initially immobile, equation (19), up to a factor τ_m/τ_{im} . Therefore, we arrive at the total density for short to intermediate times

$$n_{tot}(x, t) \sim \left(1 - \frac{t}{\tau_{im}}\right) \delta(x) + \frac{\exp\left(\frac{vx - v|x|}{2D}\right)}{2v\tau_{im}} \times \left[1 + \operatorname{erf}\left(\frac{vt - |x|}{\sqrt{4Dt}}\right) + \exp\left(\frac{v|x|}{D}\right) \left(\operatorname{erf}\left(\frac{vt + |x|}{\sqrt{4Dt}}\right) - 1\right)\right] \quad (31)$$

for $t \ll \tau_m, \tau_{im}$. The asymptote of the second summand corresponding to the mobile density in expression (31) is shown in figure 7 as the blue dashed line, which nicely matches the simulations and the Laplace inversions for $t = 10^{-3}$ and $t = 10^{-1}$. We note that $n_{tot}(x, t)$ is always normalised, $\int_{-\infty}^{\infty} n_{tot}(x, t) dx = 1$, by construction. The same arguments as presented for initially mobile tracers explain the uniform density that appears at intermediate time scales for $\tau_v \ll t \ll \tau_m, \tau_{im}$, corresponding to the second panel in figure 7. In the immobilisation dominated intermediate time domain $\tau_m \ll t \ll \tau_{im}$ the Laplace distribution with additional δ -peak

$$n_{tot}(x, t) = \frac{t}{\tau_{im}} \frac{\exp\left(\frac{vx}{2D}\right)}{\sqrt{v^2\tau_m^2 + 4D\tau_m}} \exp\left(-\sqrt{v^2\tau_m^2 + 4D\tau_m} \frac{|x|}{2D\tau_m}\right) + \left(1 - \frac{t}{\tau_{im}}\right) \delta(x) \quad (32)$$

emerges with the same scale parameter as for initially mobile tracers (23). The prefactor of the asymmetric Laplace distribution is now t/τ_{im} , and this asymmetric Laplace distribution is shown in figure 7 as the grey dashed line. The long-time limit does not depend on the initial conditions and follows the same density as the initially mobile tracers, equation (17), as shown by the red dashed line in figure 7 at $t = 10^4$.

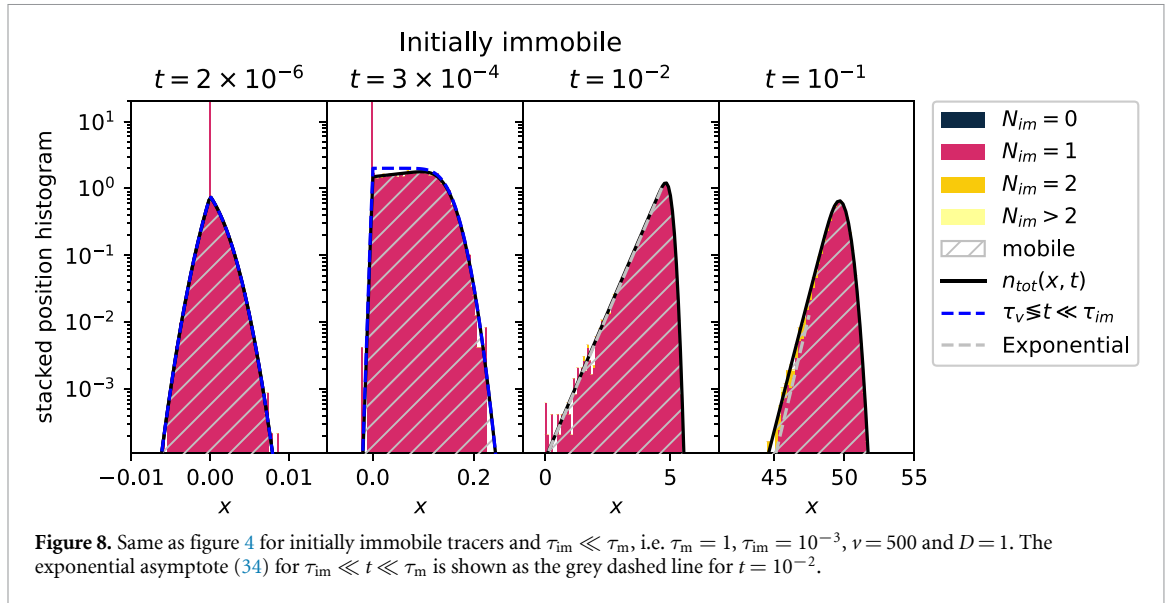


Figure 8. Same as figure 4 for initially immobile tracers and $\tau_{im} \ll \tau_m$, i.e. $\tau_m = 1$, $\tau_{im} = 10^{-3}$, $\nu = 500$ and $D = 1$. The exponential asymptote (34) for $\tau_{im} \ll t \ll \tau_m$ is shown as the grey dashed line for $t = 10^{-2}$.

4.2. Density for short immobilisations

We now consider short immobilisations, $\tau_m \ll \tau_{im}$. At short to intermediate time scales $t \ll \tau_{im} \ll \tau_m$, at which t can be shorter or longer than τ_v , the same expression (31) holds as for long immobilisations. This can be seen in figure 8, where the asymptote (31) is shown as the blue dashed line. We find excellent agreement between the histogram based on the simulations and the density (31) for $t \ll \tau_{im}, \tau_m$, see the first and second panels in figure 8 for $t = 2 \times 10^{-6}$ and $t = 3 \times 10^{-4}$, respectively. In contrast to the case $\nu = 0$ in [54], a new regime $\tau_{im} \ll t \ll \tau_m$ emerges, that we call *advection induced subdiffusion*. The total density follows an exponential distribution, as can be seen from the linear shape of the density in the semi-log plot for $t = 10^{-2}$. To explain this shape we solve the model equations (3) for the advection induced subdiffusion regime times $t \ll \tau_m$, where t can be longer or shorter than τ_v . This produces the total density

$$n_{tot}(x, t) \sim \delta(x)e^{-t/\tau_{im}} + \int_0^t \frac{e^{-t'/\tau_{im}} \exp\left(-\frac{(x-vt')^2}{4Dt'}\right)}{\tau_{im} \sqrt{4\pi Dt'}} dt', \text{ for } t \ll \tau_m, \quad (33)$$

where the integral is identical to expression (25) for immobile tracers that were initially mobile. We obtain the expression

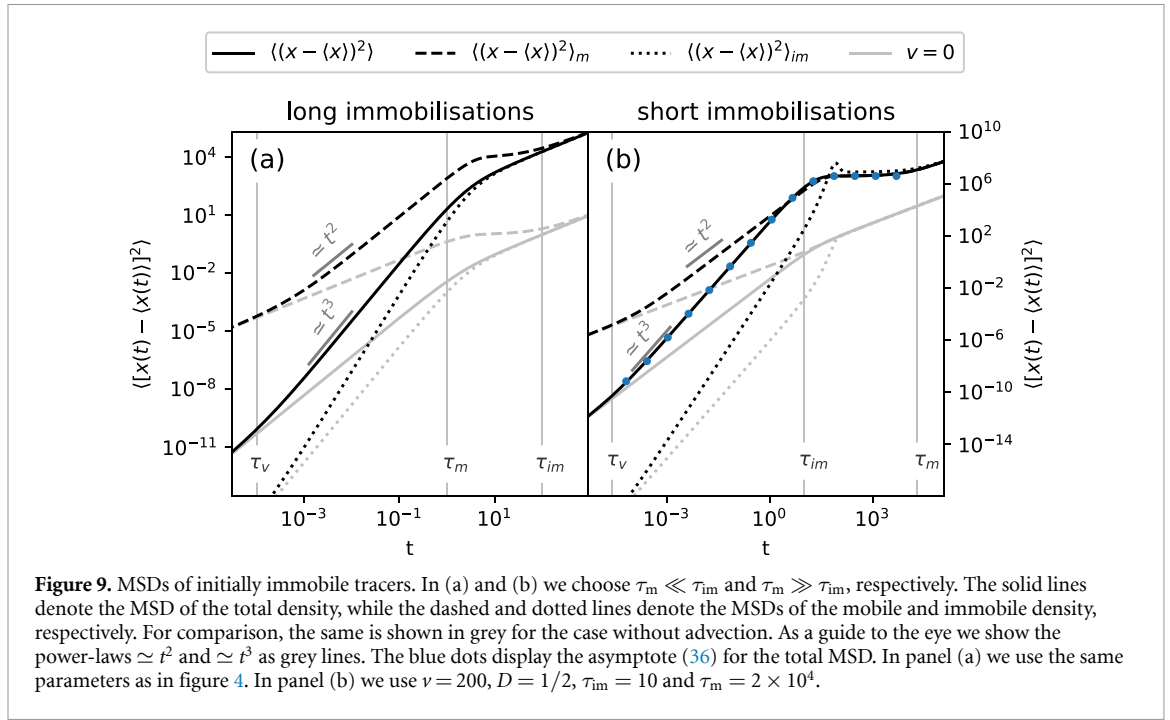
$$n_{tot}(x, t) \sim \delta(x) \exp\left(-\frac{t}{\tau_{im}}\right) + \begin{cases} \frac{1}{v\tau_{im}} \exp\left(\frac{x}{v\tau_{im}} - \frac{t}{\tau_{im}}\right) & \text{for } 0 < x \ll vt \\ 0 & \text{otherwise} \end{cases}, \quad (34)$$

for $v^2\tau_{im} \gg D$ and $t \ll \tau_m$. This comes as no surprise, as in both cases we have the same Gaussian propagator, in which the tracers have varying immobile durations. In the case of initially mobile tracers the immobile duration stems from an immobilisation at $t > 0$. In the present case of initially immobile tracers the immobile duration arises from the slow release at the origin at $t = 0$. In both cases the immobile duration is drawn from an exponential distribution with mean τ_{im} . The first term in (34) corresponds to initially immobile tracers that have not mobilised up to time t . The second term accounts for the slow release with rate $\tau_{im}^{-1} \exp(-t/\tau_{im})$ and motion in the mobile zone with advection only. The exponential distribution (34) is shown in figure 8 at $t = 2 \times 10^{-2}$ as the grey dashed line, and we find good agreement with the Laplace inversion of $n_{tot}(x, s)$ and simulations.

4.3. Mean squared displacement

We now analyse the MSD of the total density. In appendices E.2.1 and E.2.2 we analyse the MSD of the immobile and mobile density, respectively. We show the MSDs for long and short immobilisations in panels (a) and (b) of figure 9, respectively. From a series expansion of the MSD at $t = 0$ we obtain the asymptotic MSD at short to intermediate times,

$$\langle [x(t) - \langle x(t) \rangle]^2 \rangle \sim \frac{Dt^2}{\tau_{im}} + \frac{v^2}{3\tau_{im}} t^3, \text{ for } t \ll \tau_m, \tau_{im}, \quad (35)$$



in which t can be smaller or larger than τ_v . We compare the asymptote (35) to the full expression of the MSD in figure E2(b) and find very nice agreement. At short times $t \ll \tau_v$, the quadratic term dominates and we observe the same MSD as in the case without advection. This can be seen in figures 9(a) and (b). At intermediate times $\tau_v \ll t \ll \tau_m, \tau_{im}$ the cubic term in the asymptotic MSD (35) dominates. As shown in figure 9 the cubic scaling emerges for short and long immobilisations.

Now we go to the case of short immobilisation, $\tau_{im} \ll \tau_m$, for which advection induced subdiffusion emerges for $\tau_{im} \ll t \ll \tau_m$. As described in section 4.2, the total density follows an exponential distribution (34) and a δ -peak at the origin for $\tau_v \ll t \ll \tau_m$. The MSD of that distribution is given by

$$\langle [x(t) - \langle x(t) \rangle]^2 \rangle = v^2 \tau_{im} \left(\tau_{im} - 2t \exp\left(-\frac{t}{\tau_{im}}\right) - \tau_{im} \exp\left(-2\frac{t}{\tau_{im}}\right) \right), \quad (36)$$

for $\tau_v \ll t \ll \tau_m$ and $\tau_{im} \ll \tau_m$, which is shown in figure 9(b) as the blue line. From expression (36) we recover the intermediate time asymptote

$$\langle [x(t) - \langle x(t) \rangle]^2 \rangle \sim \frac{v^2 t^3}{3\tau_{im}}, \text{ for } \tau_v \ll t \ll \tau_{im}, \quad (37)$$

implying the same cubic scaling for $\tau_v \ll t \ll \tau_{im}$ as we found from the series expansion of the full MSD (35) for the advection dominated regime. This can be seen in the MSD in figure 9(b). The cubic scaling of the MSD emerges in the domain $\tau_v \ll t \ll \tau_m, \tau_{im}$, which limits the parameters to $\tau_v \ll \tau_m, \tau_{im}$. In terms of the Péclet number this implies $Pe \gg 1$ for long immobilisations $\tau_m \ll \tau_{im}$ and $Pe \gg \tau_m/\tau_{im}$ for short immobilisations $\tau_{im} \ll \tau_m$. A detailed discussion of the parameter regimes and the coexistence of the plateau regime is presented in appendix J.

In the advection induced subdiffusion domain the MSD (36) reaches the plateau value

$$\langle [x(t) - \langle x(t) \rangle]^2 \rangle \sim v^2 \tau_{im}^2, \text{ for } \tau_{im} \ll t \ll \tau_m. \quad (38)$$

These two anomalous scaling regimes shown in figure 9(b), namely, the cubic scaling and the plateau behaviour can be explained as follows. For $\tau_v \ll t \ll \tau_{im}$ the MSD grows due to the slow release and fast advection, where the spread due to diffusion is negligible. When all tracers mobilised at $t \gg \tau_{im}$, this spread due to advection vanishes, and the distribution moves along the direction of advection without changing the

Table 1. Main results of anomalous scaling of the MSD. In the second column the short-time asymptotes of the total density's MSD is shown for initially mobile and initially immobile tracers. The cubic term dominates for the time regime given in the third column, with $\tau_v = 2D/v^2$ and $\tau_* = \sqrt{3\tau_v\tau_m}$. In the fourth column the time regimes of the plateaus are given. For initially immobile tracers this advection induced subdiffusion occurs for large Péclet numbers only.

tracers initially	$t \ll \tau_m, \tau_{im}$	cubic regime	plateau regime
mobile	$2Dt + \frac{v^2}{3\tau_m} t^3$	$\tau_* \ll t \ll \tau_m, \tau_{im}$	$\tau_m \ll t \ll \tau_{im}$
immobile	$\frac{D}{\tau_{im}} t^2 + \frac{v^2}{3\tau_{im}} t^3$	$\tau_v \ll t \ll \tau_m, \tau_{im}$	$\tau_{im} \ll t \ll \tau_m$ for $Pe \gg \frac{\tau_m}{\tau_{im}}$

shape significantly. This explains the plateau in the MSD for $\tau_{im} \ll t \ll \tau_m$. We highlight that this advection induced subdiffusion is a new behaviour compared to the case without advection. For comparison, we show the MSD for $v = 0$ in figure 9(b) as the grey solid line. It crosses over from the short-time scaling $\sim Dt^2/\tau_{im}$ to the long-time asymptote $\sim 2D_{\text{eff}}t$ without any intermediate regime.

5. Conclusion

We analysed the densities along with the first and second moments of the MIM with exponential Poissonian switching between the mobile and immobile states in the presence of a drift velocity v . The whole dynamic is characterised by the mean mobile duration τ_m , the mean immobile duration τ_{im} and the time scale $\tau_v = 2D/v^2$, which is related to the Péclet number $Pe = \tau_m/\tau_v$. For $t \ll \tau_v$ advection plays a negligible role and the process is diffusion dominated, yielding the same results as in [54], where the diffusion regimes were analysed for the advection-free case. In order to highlight the role of advection we choose $\tau_v \ll \tau_{im}, \tau_m$, for which an advection dominated regime emerges for $\tau_v \ll t \ll \tau_m, \tau_{im}$. Relatively high Péclet numbers can be achieved in microfluidic setups and in certain geophysical systems. The first moment is proportional to the second moment of the advection-free model, as shown by the second Einstein relation. The second moment of the advection-free model has been discussed in detail in [54]. Therefore, we here concentrated on the discussion of the MSD. In general, for any fraction of initially mobile tracers and an arbitrary fraction τ_{im}/τ_m , we found the same long-time behaviour for $t \gg \tau_m, \tau_{im}$. The total density follows a Gaussian with an effective advection speed $v_{\text{eff}} = v\tau_m/(\tau_m + \tau_{im})$ and an effective diffusivity $D_{\text{eff}} = D\frac{\tau_m}{\tau_m + \tau_{im}} + v^2\frac{\tau_m^2\tau_{im}^2}{(\tau_m + \tau_{im})^3}$. Compared to the advection v in the free phase, v_{eff} is always smaller. The effective diffusivity D_{eff} is always larger than the effective diffusivity in the advection-free case due to the velocity-dependent term. Specifically, for sufficiently high Péclet numbers the effective diffusivity can significantly exceed the diffusivity D in the mobile domain. While D_{eff} was reported before [7, 13], we here provided a physical explanation for the additional dispersion due to the variance of durations the tracers spent in the mobile state.

We analysed two specific initial conditions with fully mobile and fully immobile tracers in detail. For initially mobile tracers the advection dominated regime contains two parts. In the first part, $\tau_v \ll t \ll \tau_* = \sqrt{3\tau_v\tau_m}$, the MSD grows linearly in time. In the second part of the advection-dominated regime, $\tau_* \ll t \ll \tau_m, \tau_{im}$, the MSD grows cubically. This regime is valid for any ratio τ_{im}/τ_m . This can be seen in table 1, where we summarise the main results of the anomalous scaling of the MSD.

For long immobilisations $\tau_{im} \gg \tau_m$ for initially mobile tracers, and in the advection dominated regime, the density consists of a Gaussian shape of mobile tracers plus a spatially uniform distribution of immobilised tracers. At longer times, $\tau_m \ll t \ll \tau_{im}$, we recovered a plateau in the MSD of initially mobile tracers reported in [54], regardless of the presence of advection. In this immobilisation dominated regime the distribution follows an asymmetric Laplace distribution, which decays rapidly in the direction opposite of the advection velocity and falls off slowly in the direction of the advection velocity. In the opposite case of short immobilisations, $\tau_{im} \ll \tau_m$, the total density follows a decreasing Gaussian shape with an increasing exponential tail in the direction opposite of the advection velocity in the whole advection dominated regime $\tau_v \ll t \ll \tau_{im}$. This exponential tail is similar to what was found for CTRWs with advection [46].

For initially immobile tracers the advection-dominated regime emerges, as well. This can be seen in table 1, where the series expansion of the MSD is shown. Here, the cubic scaling of the MSD appears in the whole regime $\tau_v \ll t \ll \tau_m, \tau_{im}$ for any ratio of τ_m/τ_{im} and a sufficiently high Péclet number. This is in contrast to the advection-free case reported in [54], where the MSD is close to the Brownian case for short immobilisations, $\tau_{im} \ll \tau_m$. For such short immobilisations the density follows a growing and drifting exponential distribution with an additional peak of immobile tracers at the origin. For later times, we found an advection induced subdiffusion regime $\tau_{im} \ll t \ll \tau_m$ for high Péclet numbers and short immobilisations.

This regime has not been reported previously. Here, the density consists of an exponential distribution with fixed scale parameters, where the mean is moving at a constant speed. For long immobilisations $\tau_m \ll \tau_{im}$, the density follows a spatially uniform distribution for $\tau_v \ll t \ll \tau_m$. For completeness, we consider an equilibrium fraction of initially mobile tracers in, which naturally occur in experiments, in appendix K, where a ballistic scaling of the MSD emerges at intermediate times.

Now we put our work into some context. A CTRW with an exponential sojourn time distribution with mean τ and a Gaussian displacement density with non-zero mean μ and variance σ^2 was considered in [46]. This model may appear similar to our model with exponentially distributed residence times in the immobile state and advection–diffusion in the mobile state. However, the MSD $\langle [x(t) - \langle x(t) \rangle]^2 \rangle = \sigma^2 t / \tau + \mu^2 t / \tau$ is linear at all times for the CTRW, as shown in appendix L.1. This contrasts the anomalous scaling at intermediate times of the MSD found here. Another formulation of CTRW is the two-state CTRW, in which two transition densities are considered from which steps are drawn in an alternating way [51]. In [51] the long-time asymptotic diffusion coefficient is obtained, which matches our result for a specific choice of parameters. We also mention the case in [52] in which a CTRW is analysed, whose waiting time distribution function is the weighted sum of two exponentials. If one of the exponential distributions has a weight close to unity and a mean that is significantly shorter than τ_m , this model generates the same MSD as the MSD of the total density from the MIM. We stress that the MIM provides additional information in the form of separate mobile and immobile densities. Thus the MIM is not simply the long-space-time limit of the model in [52]. A detailed analysis of the similarities and differences between the MIM and the processes in [51, 52] deserves a separate study.

In contrast to the advection-free case of MIM, where intermittent anomalous diffusion solely arises for mobile tracers for long immobilisations, the anomalous transport behaviours reported here occur for both long and short immobilisations. A condition for this anomalous behaviour is a high Péclet number, which occurs for example in experiments with biomolecules in biosensors [38]. Short immobilisations may occur unintentionally due to unwanted binding to the surface of a flow cell or other experimental boundaries. The resulting transport will be anomalous at intermediate time scales, even if the tracers are only subject to Brownian motion with drift in the mobile state. While the anomalous diffusion and non-Gaussian densities occur at intermediate time scales only, the measurement time is finite in experiments, and the effects may therefore erroneously appear to be an asymptotic phenomenon. In conclusion, we found a variety of anomalous diffusion regimes and non-Gaussian displacement distributions at relevant intermediate time scales in a simple MIM. We emphasise that the model's simplicity is attributed to its dependency on merely two parameters in its dimensionless representation. We finally note that persistent-intermittent anomalous scaling behaviours of the MSD as reported here for seemingly simple Poissonian mobile–immobile dynamics may be relevant for numerous experimental settings. Such scenarios should therefore be included in contemporary data analysis methods by classical observables and machine learning approaches [67–69].

Data availability statement

No new data were created or analysed in this study.

Acknowledgments

We acknowledge funding from the German Science Foundation (DFG, Grant No. ME 1535/12-1). AVC acknowledges the support of the Polish National Agency for Academic Exchange (NAWA).

Appendix A. Solving the MIM model in Fourier-Laplace space

We apply the Fourier–Laplace transform

$$f(k, s) = \int_{-\infty}^{\infty} \int_0^{\infty} e^{-st + ikx} f(x, t) dt dx \quad (\text{A.1})$$

to equations (3) and obtain the expressions

$$n_m(k, s) = \left(f_m^0 + f_{im}^0 \frac{1}{1 + s\tau_{im}} \right) \frac{1}{\phi(s) - ik_x v + k^2 D} \quad (\text{A.2})$$

$$n_{im}(k, s) = f_{im}^0 \frac{\tau_{im}}{1 + s\tau_{im}} + \frac{\tau_{im}/\tau_m}{1 + s\tau_{im}} \left(f_m^0 + f_{im}^0 \frac{1}{1 + s\tau_{im}} \right) \frac{1}{\phi(s) - ikv + k^2D} \tag{A.3}$$

as well as

$$\begin{aligned} n_{tot}(k, s) &= n_m(k, s) + n_{im}(k, s) \\ &= \frac{f_m + f_{im}^0 \frac{1}{1 + s\tau_{im}}}{s} \frac{\phi(s)}{\phi(s) - ik_x v + k^2 D} + f_{im}^0 \frac{\tau_{im}}{1 + s\tau_{im}} \end{aligned} \tag{A.4}$$

with $\phi(s) = s[1 + \tau_{im}\tau_m^{-1}/(1 + s\tau_{im})]$. Fourier inversion directly produces expressions (4) to (6).

From the densities (A.2) to (A.4) we obtain the p th moment ($p \in \mathbb{N}$)

$$(-i)^p \frac{\partial^p}{\partial k^p} n_{tot}(k, s) \Big|_{k=0} = \langle x^p(s) \rangle, \tag{A.5}$$

in Laplace space. In order to obtain the mobile and immobile moments, we first calculate the non-normalised moments

$$(-i)^p \frac{\partial^p}{\partial k^p} n_j(k, s) \Big|_{k=0} = \langle x^p(s) \rangle_{j,u} \tag{A.6}$$

with $j \in \{m, im, tot\}$. We then normalise the moment (A.6) in the time-domain with the fractions of mobile and immobile densities,

$$f_m(t) = \frac{\tau_m}{\tau_m + \tau_{im}} + \frac{f_m^0 \tau_{im} - f_{im}^0 \tau_m}{\tau_m + \tau_{im}} \exp(-[\tau_m^{-1} + \tau_{im}^{-1}]t), \tag{A.7}$$

$$f_{im}(t) = \frac{\tau_{im}}{\tau_m + \tau_{im}} - \frac{f_m^0 \tau_{im} - f_{im}^0 \tau_m}{\tau_m + \tau_{im}} \exp(-[\tau_m^{-1} + \tau_{im}^{-1}]t), \tag{A.8}$$

which we obtain by setting $k = 0$ in the densities (A.2)–(A.3) in Fourier–Laplace space and calculating the Laplace inversion.

Appendix B. Expressions of the moments

In this section we present the exact expressions of the first and second moments, which are obtained from expression (A.6).

B.1. First moments

For mobile initial conditions we find

$$\langle x(t) \rangle_{tot, f_m^0=1} = \frac{v}{1 + \tau_{im}/\tau_m} \left[t + \frac{\tau_{im}^2/\tau_m}{1 + \tau_{im}/\tau_m} \left(1 - e^{-(\tau_m^{-1} + \tau_{im}^{-1})t} \right) \right], \tag{B.1}$$

$$\begin{aligned} \langle x(t) \rangle_{m, f_m^0=1} &= \frac{v}{(1 + \tau_{im}/\tau_m) \left(1 + \tau_{im}/\tau_m e^{-(\tau_m^{-1} + \tau_{im}^{-1})t} \right)} \left[t \left(1 + \frac{\tau_{im}^2}{\tau_m^2} e^{-(\tau_m^{-1} + \tau_{im}^{-1})t} \right) \right. \\ &\quad \left. + \frac{2\tau_{im}^2/\tau_m}{1 + \tau_{im}/\tau_m} \left(1 - e^{-(\tau_m^{-1} + \tau_{im}^{-1})t} \right) \right], \end{aligned} \tag{B.2}$$

and

$$\begin{aligned} \langle x(t) \rangle_{\text{im}, f_m^0=1} &= \frac{v}{1 - e^{-(\tau_m^{-1} + \tau_{\text{im}}^{-1})t}} \left[\frac{t}{1 + \tau_{\text{im}}/\tau_m} \left(1 - \frac{\tau_{\text{im}}}{\tau_m} e^{-(\tau_m^{-1} + \tau_{\text{im}}^{-1})t} \right) \right. \\ &\quad \left. + \frac{\tau_{\text{im}}^2/\tau_m - \tau_{\text{im}}}{(1 + \tau_{\text{im}}/\tau_m)^2} \left(1 - e^{-(\tau_m^{-1} + \tau_{\text{im}}^{-1})t} \right) \right]. \end{aligned} \quad (\text{B.3})$$

For initially immobile tracers we find

$$\langle x(t) \rangle_{\text{tot}, f_{\text{im}}^0=1} = \frac{v}{1 + \tau_{\text{im}}/\tau_m} \left[t - \frac{\tau_{\text{im}}}{1 + \tau_{\text{im}}/\tau_m} \left(1 - e^{-(\tau_m^{-1} + \tau_{\text{im}}^{-1})t} \right) \right], \quad (\text{B.4})$$

$$\begin{aligned} \langle x(t) \rangle_{\text{im}, f_{\text{im}}^0=1} &= \frac{vt}{1 + \tau_m/\tau_{\text{im}}} \frac{1 + e^{-(\tau_m^{-1} + \tau_{\text{im}}^{-1})t}}{\tau_{\text{im}}/\tau_m + e^{-(\tau_m^{-1} + \tau_{\text{im}}^{-1})t}} \\ &\quad - \frac{3v\tau_{\text{im}}^2/\tau_m}{(1 + \tau_{\text{im}}/\tau_m)^2} \frac{1 - e^{-(\tau_m^{-1} + \tau_{\text{im}}^{-1})t}}{\tau_{\text{im}}/\tau_m + e^{-(\tau_m^{-1} + \tau_{\text{im}}^{-1})t}}, \end{aligned} \quad (\text{B.5})$$

and

$$\begin{aligned} \langle x(t) \rangle_{\text{m}, f_{\text{im}}^0=1} &= \frac{v}{1 - e^{-(\tau_m^{-1} + \tau_{\text{im}}^{-1})t}} \left[\frac{t}{1 + \tau_{\text{im}}/\tau_m} \left(1 - \frac{\tau_{\text{im}}}{\tau_m} e^{-(\tau_m^{-1} + \tau_{\text{im}}^{-1})t} \right) \right. \\ &\quad \left. + \frac{\tau_{\text{im}}^2/\tau_m - \tau_{\text{im}}}{(1 + \tau_{\text{im}}/\tau_m)^2} \left(1 - e^{-(\tau_m^{-1} + \tau_{\text{im}}^{-1})t} \right) \right]. \end{aligned} \quad (\text{B.6})$$

B.2. Second moments

Consider initially mobile tracers ($f_m^0 = 1$ and $f_{\text{im}}^0 = 0$). Then we obtain

$$\begin{aligned} \langle x(t)^2 \rangle_{\text{tot}, f_m^0=1} &= \frac{2D}{1 + \tau_{\text{im}}/\tau_m} \left[t + \frac{\tau_{\text{im}}^2/\tau_m}{1 + \tau_{\text{im}}\tau_m} \left(1 - e^{-(\tau_m^{-1} + \tau_{\text{im}}^{-1})t} \right) \right] \\ &\quad + \frac{v^2 t^2 \tau_m^2}{(\tau_m + \tau_{\text{im}})^2} + \frac{\tau_{\text{im}}^2 \tau_m^2 v^2}{(\tau_{\text{im}} + \tau_m)^3} \left[2t \left(2 - e^{-(\tau_m^{-1} + \tau_{\text{im}}^{-1})t} \right) \frac{\tau_{\text{im}}}{\tau_m} \right. \\ &\quad \left. - 2 \frac{2\tau_{\text{im}}\tau_m - \tau_{\text{im}}^2}{\tau_m + \tau_{\text{im}}} + 2e^{-(\tau_m^{-1} + \tau_{\text{im}}^{-1})t} \frac{(2\tau_{\text{im}}\tau_m) - \tau_{\text{im}}^2}{\tau_m + \tau_{\text{im}}} \right] \end{aligned} \quad (\text{B.7})$$

and

$$\begin{aligned} f_m(t) \langle x(t)^2 \rangle_{\text{m}, f_m^0=1} &= \frac{2D}{(1 + \tau_{\text{im}}/\tau_m)(1 + \tau_{\text{im}}/\tau_m e^{-(\tau_m^{-1} + \tau_{\text{im}}^{-1})t})} \\ &\quad \times \left[t \left(1 + \frac{\tau_{\text{im}}^2}{\tau_m^2} e^{-(\tau_m^{-1} + \tau_{\text{im}}^{-1})t} \right) + \frac{2\tau_{\text{im}}^2/\tau_m}{1 + \tau_{\text{im}}/\tau_m} \left(1 - e^{-(\tau_m^{-1} + \tau_{\text{im}}^{-1})t} \right) \right] \\ &\quad + \frac{v^2 t^2}{(\tau_m + \tau_{\text{im}})^3} \left(\tau_m^3 + \tau_{\text{im}}^3 e^{-(\tau_m^{-1} + \tau_{\text{im}}^{-1})t} \right) \\ &\quad + \frac{6v^2 t \tau_{\text{im}}^2 \tau_m^2}{(\tau_m + \tau_{\text{im}})^4} \left(\tau_m - \tau_{\text{im}} e^{-(\tau_m^{-1} + \tau_{\text{im}}^{-1})t} \right) \\ &\quad + \frac{6v^2 \tau_{\text{im}}^3 (\tau_{\text{im}} \tau_m^3 - \tau_m^4)}{(\tau_m + \tau_{\text{im}})^5} \left(1 - e^{-(\tau_m^{-1} + \tau_{\text{im}}^{-1})t} \right), \end{aligned} \quad (\text{B.8})$$

along with

$$\begin{aligned}
 f_{\text{im}}(t)\langle x(t)^2 \rangle_{\text{im}, f_{\text{im}}^0=1} &= \frac{2D}{1 - e^{-(\tau_m^{-1} + \tau_{\text{im}}^{-1})t}} \left[\frac{t}{1 + \tau_{\text{im}}/\tau_m} \left(1 - \frac{\tau_{\text{im}}}{\tau_m} e^{-(\tau_m^{-1} + \tau_{\text{im}}^{-1})t} \right) \right. \\
 &+ \frac{\tau_{\text{im}}^2/\tau_m - \tau_{\text{im}}}{(1 + \tau_{\text{im}}/\tau_m)^2} \left(1 - e^{-(\tau_m^{-1} + \tau_{\text{im}}^{-1})t} \right) \\
 &+ \frac{2v^2\tau_{\text{im}}}{\tau_m} \left[\frac{t^2\tau_m \left(\tau_m^2 - e^{-(\tau_m^{-1} + \tau_{\text{im}}^{-1})t} \tau_{\text{im}}^2 \right)}{2(\tau_m + \tau_{\text{im}})^3} + \frac{t\tau_{\text{im}}}{(\tau_m + \tau_{\text{im}})^4} \right. \\
 &\times \left((2\tau_{\text{im}}\tau_m^3 - \tau_m^4) - e^{-(\tau_m^{-1} + \tau_{\text{im}}^{-1})t} \tau_{\text{im}}(\tau_{\text{im}}\tau_m^2 - 2\tau_m^3) \right) \\
 &\left. \left. + \frac{\tau_{\text{im}}^4\tau_m^3 - 4\tau_{\text{im}}^3\tau_m^4 + \tau_{\text{im}}^2\tau_m^5}{(\tau_m + \tau_{\text{im}})^5} \left(1 - e^{-(\tau_m^{-1} + \tau_{\text{im}}^{-1})t} \right) \right] \right]. \tag{B.9}
 \end{aligned}$$

For initially immobile tracers the moments read

$$\begin{aligned}
 \langle x(t)^2 \rangle_{\text{tot}, f_{\text{im}}^0=1} &= \frac{2D}{1 + \tau_{\text{im}}/\tau_m} \left[t - \frac{\tau_{\text{im}}}{1 + \tau_{\text{im}}/\tau_m} \left(1 - e^{-(\tau_m^{-1} + \tau_{\text{im}}^{-1})t} \right) \right] \\
 &\frac{v^2 t^2 \tau_m^2}{(\tau_{\text{im}} + \tau_m)^2} + 2 \frac{tv^2 \tau_{\text{im}}^2 \tau_m^2}{(\tau_{\text{im}} + \tau_m)^3} \left(1 - \frac{\tau_m}{\tau_{\text{im}}} + e^{-(\tau_m^{-1} + \tau_{\text{im}}^{-1})t} \right) \\
 &- 2 \frac{v^2 (2\tau_{\text{im}}^3 \tau_m^3 - \tau_{\text{im}}^2 \tau_m^4)}{(\tau_m + \tau_{\text{im}})^4} \left(1 - e^{-(\tau_m^{-1} + \tau_{\text{im}}^{-1})t} \right), \tag{B.10}
 \end{aligned}$$

$$\begin{aligned}
 f_{\text{m}}(t)\langle x(t)^2 \rangle_{\text{m}, f_{\text{im}}^0=1} &= \frac{2D}{1 - e^{-(\tau_m^{-1} + \tau_{\text{im}}^{-1})t}} \left[\frac{t}{1 + \tau_{\text{im}}/\tau_m} \left(1 - \frac{\tau_{\text{im}}}{\tau_m} e^{-(\tau_m^{-1} + \tau_{\text{im}}^{-1})t} \right) \right. \\
 &+ \frac{\tau_{\text{im}}^2/\tau_m - \tau_{\text{im}}}{(1 + \tau_{\text{im}}/\tau_m)^2} \left(1 - e^{-(\tau_m^{-1} + \tau_{\text{im}}^{-1})t} \right) \\
 &+ \frac{v^2 t^2 \tau_m}{(\tau_m + \tau_{\text{im}})^3} \left(\tau_m^2 - \tau_{\text{im}}^2 e^{-(\tau_m^{-1} + \tau_{\text{im}}^{-1})t} \right) \\
 &+ \frac{2v^2 t \tau_{\text{im}} \tau_m^3}{(\tau_{\text{im}} + \tau_m)^4} \left(2\tau_{\text{im}} - \tau_m - e^{-(\tau_m^{-1} + \tau_{\text{im}}^{-1})t} \tau_{\text{im}} \left(\frac{\tau_{\text{im}}}{\tau_m} - 2 \right) \right) \\
 &\left. + \frac{2v^2 \tau_{\text{im}}^2 \tau_m^3 ((\tau_{\text{im}} - \tau_m)^2 - 2\tau_{\text{im}}\tau_m)}{(\tau_m + \tau_{\text{im}})^5} \left(1 - e^{-(\tau_m^{-1} + \tau_{\text{im}}^{-1})t} \right) \right] \tag{B.11}
 \end{aligned}$$

and

$$\begin{aligned}
 f_{\text{im}}(t)\langle x(t)^2 \rangle_{\text{im}, f_{\text{im}}^0=1} &= \frac{2Dt}{1 + \tau_m/\tau_{\text{im}}} \frac{1 + e^{-(\tau_m^{-1} + \tau_{\text{im}}^{-1})t}}{\tau_{\text{im}}/\tau_m + e^{-(\tau_m^{-1} + \tau_{\text{im}}^{-1})t}} \\
 &- \frac{4D\tau_{\text{im}}^2/\tau_m}{(1 + \tau_{\text{im}}/\tau_m)^2} \frac{1 - e^{-(\tau_m^{-1} + \tau_{\text{im}}^{-1})t}}{\tau_{\text{im}}/\tau_m + e^{-(\tau_m^{-1} + \tau_{\text{im}}^{-1})t}} \\
 &+ 2v^2 \frac{\tau_{\text{im}}}{\tau_m} \left[\frac{t^2 \tau_m^2}{2(\tau_m + \tau_{\text{im}})^3} \left(\tau_m + \tau_{\text{im}} e^{-(\tau_m^{-1} + \tau_{\text{im}}^{-1})t} \right) \right. \\
 &+ \frac{t\tau_{\text{im}}}{(\tau_m + \tau_{\text{im}})^4} \left((\tau_{\text{im}}\tau_m^3 - 2\tau_m^4) + e^{-(\tau_m^{-1} + \tau_{\text{im}}^{-1})t} (2\tau_{\text{im}}\tau_m^3 - \tau_m^4) \right) \\
 &\left. - \frac{3\tau_{\text{im}}^3 (\tau_{\text{im}}\tau_m^4 - \tau_m^5)}{(\tau_m + \tau_{\text{im}})^5} \left(1 - e^{-(\tau_m^{-1} + \tau_{\text{im}}^{-1})t} \right) \right]. \tag{B.12}
 \end{aligned}$$

Appendix C. Series expansion of moments

The series expansion of the MSDs is shown in table C1.

Table C1. Short to intermediate time expansions for $t \ll \tau_m, \tau_{im}$ of the MSD for different fractions of initially mobile tracers f_m^0 .

j	series of $\langle [x(t) - \langle x(t) \rangle]^2 \rangle_j$ for $t \ll \tau_m, \tau_{im}$
	$f_m^0 = 1$
tot	$2Dt - \frac{Dt^2}{\tau_m} + \left[v^2 + D \left(\frac{1}{\tau_m} + \frac{1}{\tau_{im}} \right) \right] \frac{t^3}{3\tau_m} - \left[2v^2 \left(\frac{2}{\tau_m} + \frac{1}{\tau_{im}} \right) + D \left(\frac{1}{\tau_m} + \frac{1}{\tau_{im}} \right)^2 \right] \frac{t^4}{12\tau_m}$
m	$2Dt - \frac{Dt^3}{3\tau_m\tau_{im}} + \left[\frac{v^2}{12} + D \left(\frac{1}{6\tau_{im}} - \frac{1}{6\tau_m} \right) \right] \frac{t^4}{\tau_m\tau_{im}} + \left[3v^2(\tau_{im} - \tau_m) + D \left(14 - \frac{3\tau_{im}}{\tau_m} - \frac{3\tau_m}{\tau_{im}} \right) \right] \frac{t^5}{60\tau_m^2\tau_{im}^2}$
im	$Dt + \left[\frac{v^2}{12} + D \left(\frac{1}{6\tau_{im}} - \frac{1}{6\tau_m} \right) \right] t^2 + \left[v^2 \left(2 - \frac{3\tau_m}{\tau_{im}} - \frac{3\tau_{im}}{\tau_m} \right) + 2D(\tau_{im} - \tau_m) \left(\frac{1}{\tau_{im}} + \frac{1}{\tau_m} \right)^2 \right] \frac{t^3}{720\tau_{im}\tau_m}$
	$f_{im}^0 = 1$
tot	$\frac{Dt^2}{\tau_{im}} + \frac{v^2 - D \left(\frac{1}{\tau_m} + \frac{1}{\tau_{im}} \right)}{3\tau_{im}} t^3$
m	$Dt + \left[\frac{v^2}{12} + D \left(\frac{1}{6\tau_{im}} - \frac{1}{6\tau_m} \right) \right] t^2$
im	$\frac{Dt^3}{3\tau_m\tau_{im}} + \left[\frac{v^2}{12} + D \left(\frac{1}{6\tau_{im}} - \frac{1}{6\tau_m} \right) \right] \frac{t^4}{\tau_m\tau_{im}}$

Appendix D. Details on subordination

The probability density function $P(\tau, t)$ of $\tau(t) = \int_0^t i(t') dt'$ is calculated in [23] and reads

$$P(\tau, t) = f_m^0 \sum_{q=1}^{\infty} (P_{q,q-1}^u(\tau, t) + P_{q,q}^u(\tau, t)) + f_{im}^0 \sum_{q=1}^{\infty} (P_{q,q}^b(\tau, t) + P_{q-1,q}^b(\tau, t)). \quad (D.1)$$

Here, $P_{q,r}^u(\tau, t)$ and $P_{q,r}^b(\tau, t)$ denote the probability of initially mobile and immobile tracers, respectively, to spend in total the duration τ mobile in q mobile periods. The tracer remains immobile for the total duration $t - \tau$ in r immobile periods. The expressions for $P_{q,r}^u(\tau, t)$ and $P_{q,r}^b(\tau, t)$ are given by

$$P_{q+1,q}^u(s, t) = \begin{cases} \frac{1}{\tau_{im}} \frac{1}{q!(q-1)!} \left(\frac{s}{\tau_m} \right)^q \left(\frac{t-s}{\tau_{im}} \right)^{q-1} \exp \left(-\frac{s}{\tau_m} - \frac{t-s}{\tau_{im}} \right) & \text{for } q \geq 1 \\ \exp \left(-\frac{s}{\tau_m} \right) & \text{for } q = 0 \end{cases}, \quad (D.2)$$

$$P_{q,q}^u(s, t) = \frac{1}{\tau_m} \frac{1}{((q-1)!)^2} \left(\frac{s(t-s)}{\tau_m\tau_{im}} \right)^{q-1} \exp \left(-\frac{s}{\tau_m} - \frac{t-s}{\tau_{im}} \right) \text{ for } q \geq 1, \quad (D.3)$$

$$P_{q,q}^b(s, t) = \frac{1}{\tau_{im}} \frac{1}{((q-1)!)^2} \left(\frac{s(t-s)}{\tau_m\tau_{im}} \right)^{q-1} \exp \left(-\frac{s}{\tau_m} - \frac{t-s}{\tau_{im}} \right), \quad (D.4)$$

and

$$P_{q,q+1}^b(s, t) = + \begin{cases} \frac{1}{\tau_m} \frac{1}{q!(q-1)!} \left(\frac{t-s}{\tau_{im}} \right)^q \exp \left(-\frac{s}{\tau_m} - \frac{t-s}{\tau_{im}} \right) & \text{for } q \geq 1 \\ \exp \left(-\frac{t}{\tau_{im}} \right) & \text{for } q = 0 \end{cases}. \quad (D.5)$$

In geological experiments, typically the mobile density is measured [18]. Similarly to expression (11), we obtain the mobile density

$$n_m(x, t) = \int_0^t P_m(t', t) \frac{e^{-\frac{(x-vt')^2}{4Dt'}}}{\sqrt{4\pi Dt'}} dt', \quad (D.6)$$

with the probability $P_m(t', t)$ to be mobile for a total duration t' at time t conditioned to be in the mobile phase at time t . From expression (D.1) we simply need to remove the terms with an additional immobilisation to obtain

$$P_m(s, t) = \sum_{q=1}^{\infty} (f_m^0 P_{q,q-1}^u(s, t) + f_{im}^0 P_{q,q}^b(s, t)). \quad (D.7)$$

The immobile density $n_{\text{im}}(x, y, t)$ and $P_{\text{im}}(s, t)$ can be defined analogously to expressions (D.6) and (D.7) with

$$P_{\text{im}}(s, t) = \sum_{q=1}^{\infty} (f_{\text{m}}^0 P_{q,q}^u(s, t) + f_{\text{im}}^0 P_{q-1,q}^b(s, t)). \quad (\text{D.8})$$

The subordinator $P(s, t)$ can also be obtained in another way, as we show now. Since $i(t)$ follows a telegraph process, it is easy to see that the probability density functions $P_{\text{m}}(\tau, t) \equiv P(\tau, t | i(t) = 1)$ and $P_{\text{im}}(\tau, t) \equiv P(\tau, t | i(t) = 0)$ for the operational time obey the following set of equations

$$\begin{aligned} \frac{\partial}{\partial t} P_{\text{m}}(\tau, t) &= -\frac{P_{\text{m}}(\tau, t)}{\tau_{\text{m}}} + \frac{P_{\text{im}}(\tau, t)}{\tau_{\text{im}}} - \frac{\partial}{\partial \tau} P_{\text{m}}(\tau, t), \\ \frac{\partial}{\partial t} P_{\text{im}}(\tau, t) &= \frac{P_{\text{m}}(\tau, t)}{\tau_{\text{m}}} - \frac{P_{\text{im}}(\tau, t)}{\tau_{\text{im}}}, \end{aligned} \quad (\text{D.9})$$

where $P_{\text{m}}(\tau, t)$ and $P_{\text{im}}(\tau, t)$ denote the subordinator $P(\tau, t)$ conditioned on the tracer being mobile or immobile at time t , respectively, with $P(\tau, t) = P_{\text{m}}(\tau, t) + P_{\text{im}}(\tau, t)$. Double Laplace transform $\int_0^{\infty} dt \int_0^{\infty} d\tau f(\tau, t) \exp(-st - u\tau) = f(u, s)$ of $P(\tau, t)$ yields

$$P(u, s) = \frac{f_{\text{m}}^0 + f_{\text{im}}^0 \frac{1}{1+s\tau_{\text{im}}}}{s} \frac{\phi(s)}{\phi(s) + u} + f_{\text{im}}^0 \frac{\tau_{\text{im}}}{1 + s\tau_{\text{im}}}, \quad (\text{D.10})$$

with $\phi(s) = s[1 + \tau_{\text{im}}\tau_{\text{m}}^{-1}/(1 + s\tau_{\text{im}})]$. From $P(u, s)$ (D.10) we obtain the first and second moments in Laplace space

$$\langle \tau^p(s) \rangle = (-1)^p \left. \frac{\partial^p}{\partial u^p} P(u, s) \right|_{u=0}, \quad (\text{D.11})$$

for $p = 1$ and $p = 2$, respectively. We do not provide the lengthy expressions in time domain here. In the long-time $t \gg \tau_{\text{m}}, \tau_{\text{im}}$ the first moment is given by $\langle \tau(t) \rangle \sim t\tau_{\text{m}}/(\tau_{\text{m}} + \tau_{\text{im}})$ and the second central moment is given by $\langle [\tau(t) - \langle \tau(t) \rangle]^2 \rangle \sim 2\tau_{\text{m}}^2\tau_{\text{im}}^2/(\tau_{\text{m}} + \tau_{\text{im}})^3 t$. Laplace-inversion of $P(u, s)$ (D.10) gives the expression

$$P(\tau, s) = \frac{f_{\text{m}}^0 + f_{\text{im}}^0 \frac{1}{1+s\tau_{\text{im}}}}{s} \phi(s) \exp(-\tau\phi(s))\theta(s) + f_{\text{im}}^0 \delta(\tau) \frac{\tau_{\text{im}}}{1 + s\tau_{\text{im}}}, \quad (\text{D.12})$$

with the Heaviside step function $\theta(s)$.

Appendix E. Additional figures and asymptotes of the MSD

In this section we show additional figures of the MSD and develop asymptotic expressions of the mobile and immobile densities. In figure E1 the MSD is shown in addition to the instantaneous diffusion exponent $\alpha(t)$ for initially mobile tracers. For instance the cubic scaling can be seen in panels (c) and (d), where $\alpha(t)$ takes on values close to three for extended periods. In figure E2 we compare the expressions obtained for intermediate time scales to the exact expressions of the MSD.

E.1. Mobile initial conditions

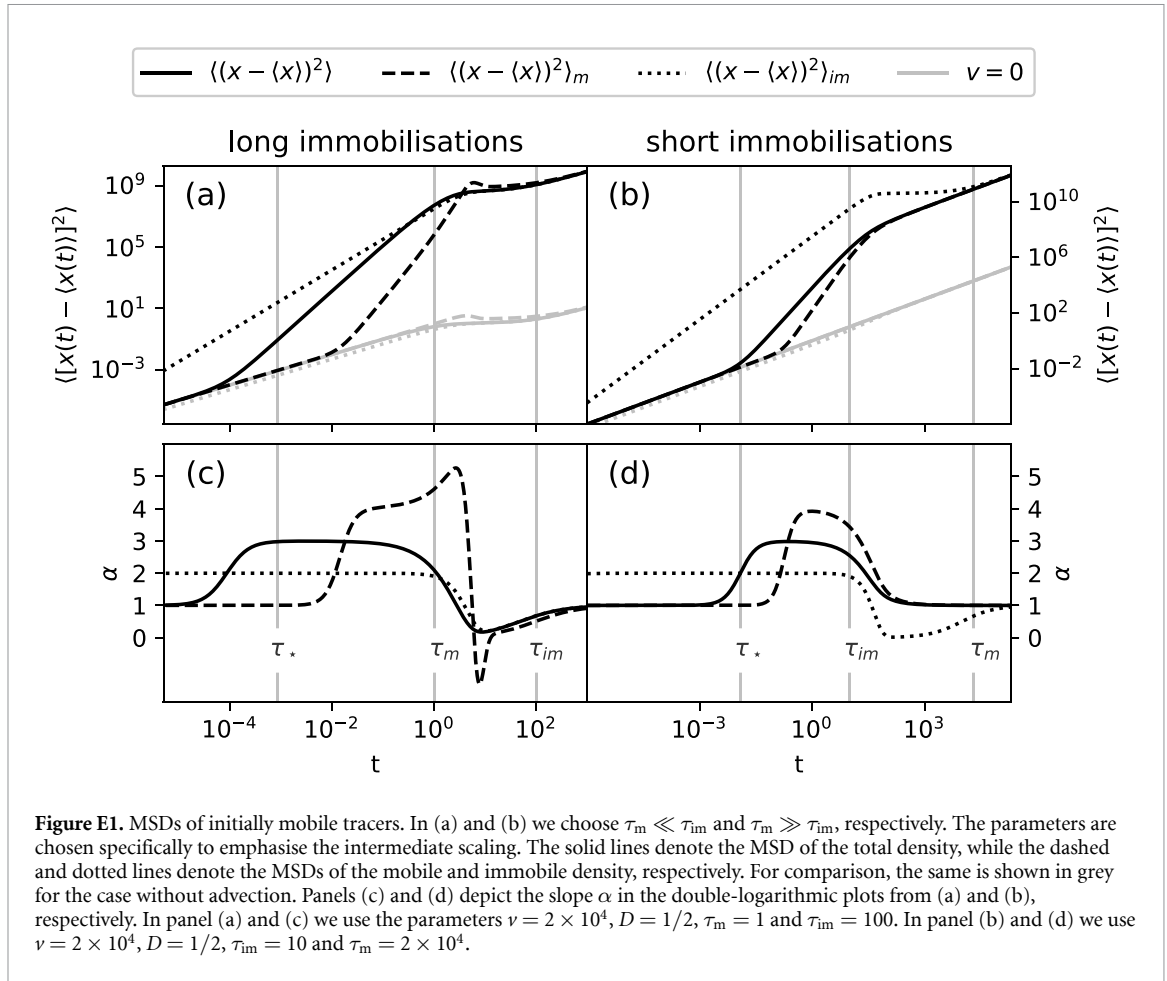
We assume initially mobile tracers and obtain asymptotic expressions in sections appendices E.1.1 and E.1.2.

E.1.1. MSD of the immobile density

Now we turn to the MSD of the immobile density. A series expansion of the exact MSD produces

$$\langle [x(t) - \langle x(t) \rangle]_{\text{im}}^2 \rangle \sim Dt + \frac{v^2}{12} t^2, \text{ for } t \ll \tau_{\text{m}} \ll \tau_{\text{im}}. \quad (\text{E.1})$$

Expression (E.1) implies a ballistic scaling of the immobile MSD for $6\tau_v \ll t \ll \tau_{\text{m}}, \tau_{\text{im}}$. This matches the MSD of the uniform distribution (20) of $n_{\text{im}}(x, t)$ shown in figure 4 where the right border moves at a constant speed. The immobile MSD with the ballistic scaling is shown in figure 6(a) as the dotted line.



Panel (c) depicts the anomalous diffusion exponent α , which is close to two for $6\tau_v \ll t \ll \tau_m$. Figure 6(a) shows the MSD of the mobile density as a dashed black line. For almost all times $t \ll \tau_m$ it coincides with $2Dt$ corresponding to the case without advection and Brownian diffusion. The reason for this is that at $t < \tau_m \ll \tau_{im}$ almost all mobile tracers have never immobilised, as shown in figure 4.

E.1.2. MSD of the mobile density

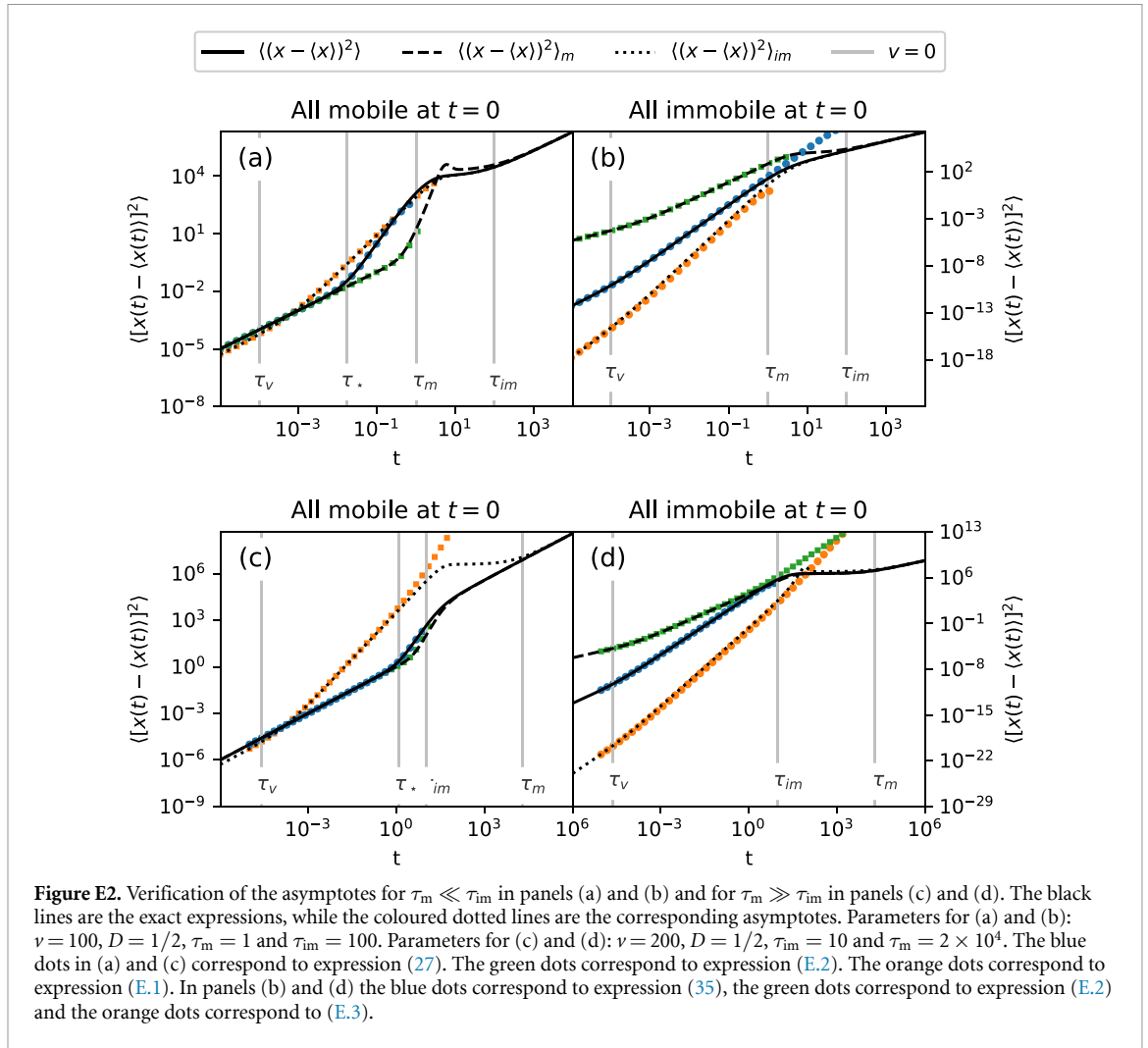
The MSD of the mobile density has the series expansion

$$\langle [x(t) - \langle x(t) \rangle]^2 \rangle = 2Dt + \frac{v^2}{12\tau_m\tau_{im}}t^4, \text{ for } t \ll \tau_m, \tau_{im}. \quad (\text{E.2})$$

The short-time behaviour $2Dt$ dominates up to $(2D\tau_m\tau_{im}/v^2)^{1/3}$, as shown in figures 6(a) and (b). The time scale $(2D\tau_m\tau_{im}/v^2)^{1/3}$ is very close to τ_m in panel (a) and close to τ_{im} in panel (b), therefore the t^4 scaling is not observed in figure 6. In the appendix in figure E1(a), we choose a higher Péclet number, for which the t^4 scaling is distinct. After τ_m the MSD has a peak and decreases afterwards for some time. This can be explained similarly to the advection free case in [54]. Up to τ_m , most of the mobile density consists of mobile tracers that have never immobilised. This can be seen in the histogram for $t = 0.1$ in figure 4, where most of the mobile density follows a Gaussian which is coloured black corresponding to zero immobilisation events $N_{im} = 0$. When the mobile density mostly consists of tracers that were immobile once the MSD decreases because the leading Gaussian peak is missing.

E.2. Immobile initial conditions

We assume initially immobile tracers and obtain asymptotic expressions in sections appendices E.2.1 and E.2.2.



E.2.1. MSD of the immobile density

From a series expansion of the immobile MSD we obtain the short to intermediate time asymptote of the immobile population,

$$\langle [x(t) - \langle x(t) \rangle]^2 \rangle_{im} \sim \frac{Dt^3}{3\tau_{im}\tau_m} + \frac{\nu^2}{12\tau_{im}\tau_m} t^4, \text{ for } t \ll \tau_m, \tau_{im}, \quad (E.3)$$

where t can be shorter or longer than τ_v . In figure E2(b) we verify this asymptote and it shows good agreement with the full analytical solution. For a high Péclet number $Pe = \frac{\nu^2 \tau_m}{2D} \gg 1$ the quartic term in the asymptotic MSD (E.3) dominates for $\tau_v \ll t \ll \tau_m, \tau_{im}$, as shown in figures 9(a) and (b).

E.2.2. MSD of the mobile density

The MSD of the mobile density with immobile initial conditions is the same as the MSD (E.1) of the immobile density with mobile initial conditions [54]. In the long-time limit $t \gg \tau_v, \tau_m, \tau_{im}$, the MSD is linear with effective diffusion coefficient (15).

Appendix F. Calculations for long immobilisations

We consider $s\tau_{im}, s\tau_m \gg 1$ in $n_{im}(x, s)$ (5), and find the expression

$$n_{im}(x, s) = \left(\frac{1}{s\tau_m} \right) \frac{\exp\left(\frac{\nu x}{2D}\right)}{\sqrt{\nu^2 + 4\phi(s)D}} \exp\left(-\sqrt{\nu^2 + 4\phi(s)D} \frac{|x|}{2D}\right), \quad (F.1)$$

which corresponds in time-domain to the integral

$$n_{\text{im}}(x, t) \sim \frac{1}{\tau_{\text{m}}} \int_0^t dt' \frac{\exp\left(-\frac{(x-vt')^2}{4Dt'}\right)}{\sqrt{4\pi Dt'}} \quad (\text{E.2})$$

$$\sim \frac{\exp\left(\frac{vx-v|x|}{2D}\right)}{2v\tau_{\text{m}}} \left[1 + \operatorname{erf}\left(\frac{tv-|x|}{\sqrt{4Dt}}\right) + \exp\left(\frac{v|x|}{D}\right) \left(\operatorname{erf}\left(\frac{tv+|x|}{\sqrt{4Dt}}\right) - 1 \right) \right]. \quad (\text{E.3})$$

The integral (E.2) has the physical interpretation of mobile tracers following a Gaussian and immobilising with the constant rate $1/\tau_{\text{m}}$.

Appendix G. Density with short immobilisations

For $t \ll \tau_{\text{m}}$, the fraction t/τ_{m} of mobile tracers is trapped for a short period τ drawn from $\gamma(\tau) = \exp(-\tau/\tau_{\text{im}})/\tau_{\text{im}}$. This is shown as the red area in figure 5 denoting one immobilisation. Hence, these tracers were mobile for a total period of $t - \tau$. We convolute this with the propagator for advection diffusion and obtain the expression

$$\begin{aligned} a(x, t) &= \int_0^t \frac{\exp\left(-\frac{(x-vt')^2}{4Dt'}\right)}{\sqrt{4\pi Dt'}} e^{-(t-t')/\tau_{\text{im}}} dt' \\ &= \frac{\exp\left(-\frac{t}{\tau_{\text{im}}} + \frac{vx}{2D}\right)}{2\sqrt{v^2 - \frac{4D}{\tau_{\text{im}}}}} \left(\exp\left(-|x|\sqrt{\frac{v^2}{4D^2} - \frac{1}{D\tau_{\text{im}}}}\right) \operatorname{erfc}\left(\frac{x-t\sqrt{v^2 - \frac{4D}{\tau_{\text{im}}}}}{2\sqrt{Dt}}\right) \right. \\ &\quad \left. - \exp\left(|x|\sqrt{\frac{v^2}{4D^2} - \frac{1}{D\tau_{\text{im}}}}\right) \operatorname{erfc}\left(\frac{x+t\sqrt{v^2 - \frac{4D}{\tau_{\text{im}}}}}{2\sqrt{Dt}}\right) \right) \end{aligned} \quad (\text{G.1})$$

with the complimentary error function $\operatorname{erfc}(x)$. Note that (G.1) is also valid for $v^2 < 4D/\tau_{\text{im}}$, i.e. also for the case without advection. The seemingly imaginary parts cancel out. Expression (G.1) can be rewritten as $a(x, t) = \operatorname{Im}(\operatorname{erf}(\frac{ibt-|x|}{\sqrt{Dt}}) \exp(-ib|x|/2D)) - \sin(b|x|/2D)/b$, which is strictly positive with $ib = \sqrt{v^2 - 4D/\tau_{\text{im}}}$, and it does not oscillate. The $-\sin(\dots)$ rather removes the oscillatory part of the $\operatorname{Im}(\exp(-ib|x|/2D))$ and the error function approaches unity for large x .

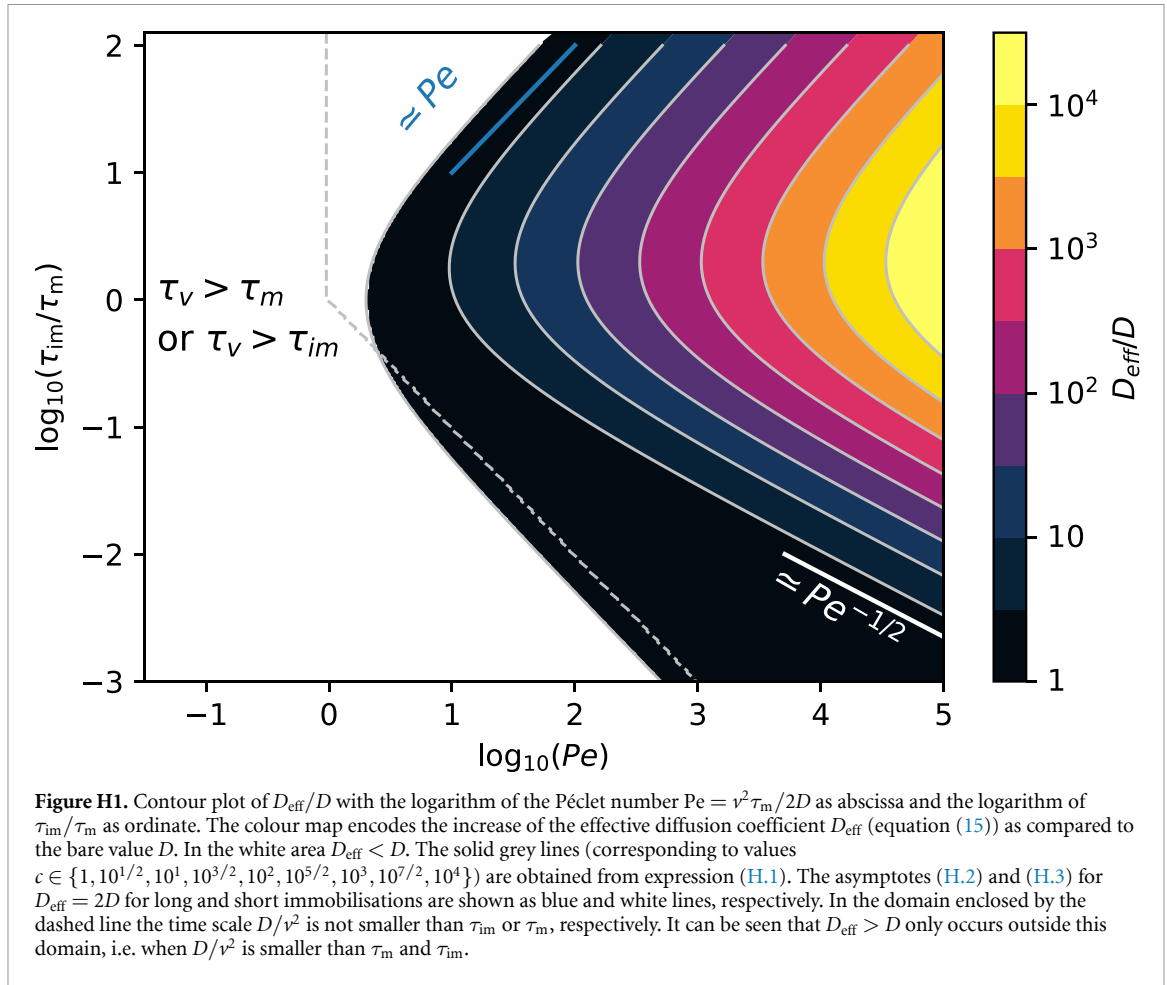
Appendix H. Dependence of D_{eff} on the model parameters

We now analyse the dependence of the effective diffusion coefficient on the model parameters. In section 2.3 we show that only two dimensionless parameters characterise the model, namely the Péclet number and $\tau_{\text{im}}/\tau_{\text{m}}$. We use the decadic logarithms of these parameters as the abscissa and ordinate in figure H1. The logarithmic colour map encodes the ratio D_{eff}/D for $D_{\text{eff}} > D$. Outside that region D_{eff} is smaller than D , as in the case without advection in [54]. For high Péclet numbers D_{eff} takes on high values depending on $\tau_{\text{im}}/\tau_{\text{m}}$. Now we analyse this dependence in more detail. For $D > 0$ we now analyse the ratio $D_{\text{eff}}/D = c(\text{Pe}, \tau_{\text{m}}/\tau_{\text{im}})$, that depends on Pe and $\tau_{\text{m}}/\tau_{\text{im}}$. For $c \geq 1$ we find the expression

$$\text{Pe} = \frac{c-1}{2} \left(1 + \frac{\tau_{\text{m}}}{\tau_{\text{im}}} \right)^2 + \frac{c}{2} \left(1 + \frac{\tau_{\text{m}}}{\tau_{\text{im}}} \right) \left(1 + \frac{\tau_{\text{im}}}{\tau_{\text{m}}} \right), \quad (\text{H.1})$$

which is the Péclet number as a function of $\tau_{\text{im}}/\tau_{\text{m}}$. It is shown for a range of c values in figure H1 as solid grey lines and matches the colour plot. We obtain the asymptotes

$$\text{Pe} \sim c \frac{\tau_{\text{im}}}{2\tau_{\text{m}}}, \text{ for } \tau_{\text{m}} \ll \tau_{\text{im}}, \quad (\text{H.2})$$



and

$$Pe \sim \begin{cases} \frac{\tau_m}{2\tau_{\text{im}}}, & \text{for } \tau_m \gg \tau_{\text{im}} \text{ and } c = 1 \\ \frac{c-1}{2(\tau_{\text{im}}/\tau_m)^2}, & \text{for } \tau_m \gg \tau_{\text{im}} \text{ and } c > 1 \end{cases}, \quad (\text{H.3})$$

from expression (H.1). The asymptote (H.2) is shown as the blue line at the top of the map in figure H1. For the lower bound in the map we choose $c = 2$ and depict the asymptote $Pe^{-1/2}$ as a white line in figure H1. Both asymptotes are parallel to the exact expressions shown as grey lines.

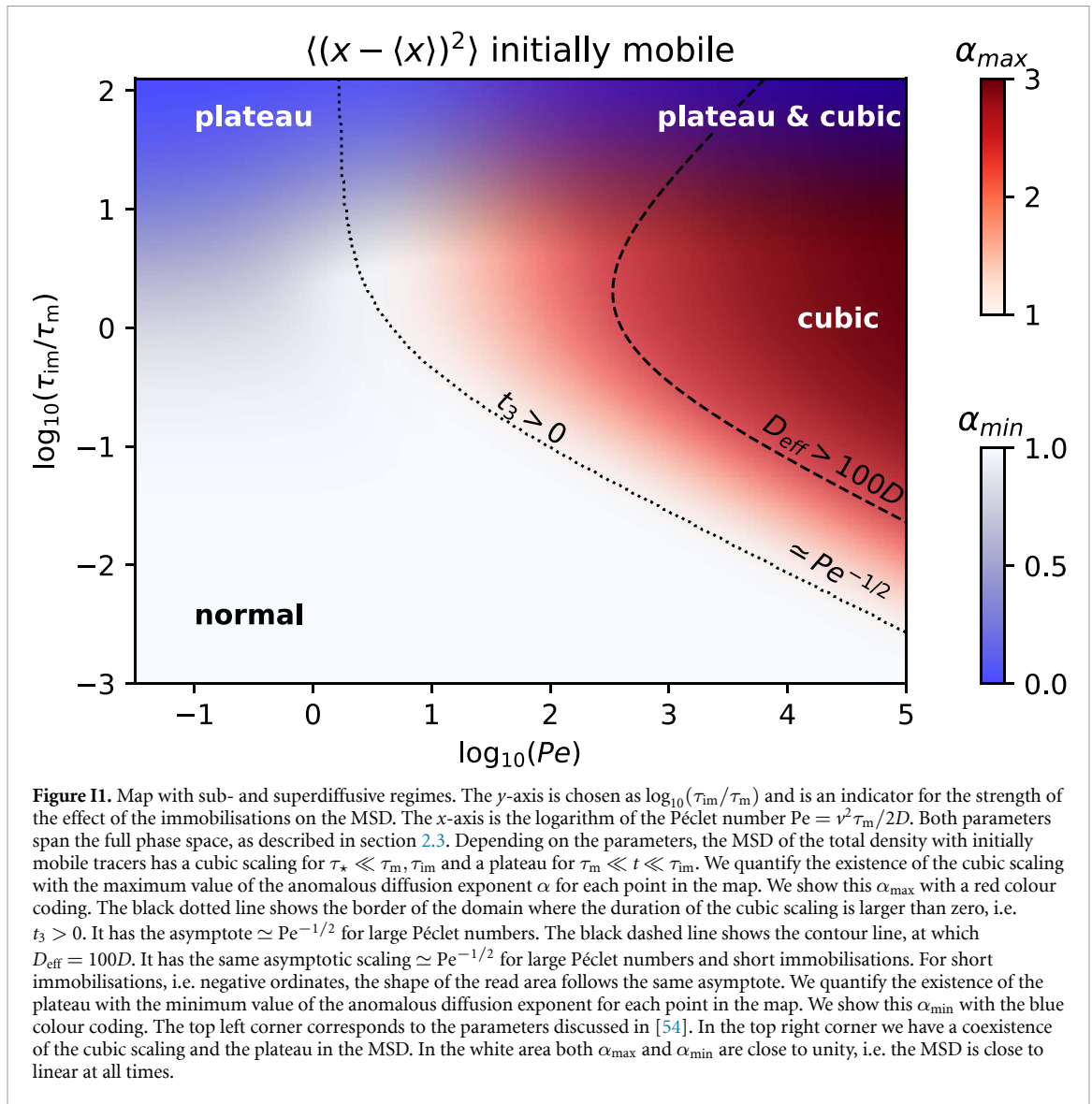
Appendix I. Parameter regimes for anomalous diffusion for initially mobile tracers

I.1. Parameter regimes for superdiffusion

Here we analyse for which parameter regimes the cubic scaling (27) of the total MSD appears for initially mobile tracers. First, long immobilisations are assumed in section appendix I.2 $\tau_m \ll \tau_{\text{im}}$, followed by short immobilisations in section appendix I.3.

I.2. Long immobilisations

A necessary condition for the cubic regime to emerge is that the lower bound τ_* of the time regime is smaller than the upper bound τ_m . We define t_3 as the duration between the upper and lower bound. This restricts the parameter space in which the cubic regime appears to positive values of the time difference t_3 . As shown in section 2.3, the whole parameter space can be spanned by the Péclet number $Pe = v^2\tau_m/2D$ and the ratio τ_{im}/τ_m . We use the decadic logarithm of these quantities as axis for a map in figure I1, similar to figure H1. The border of the region with $t_3 > 0$ in the top right of figure H1 is shown as a black dotted line. We notice that $Pe > 1$ is a necessary condition for $t_3 > 0$. We analyse the parameter space for $\tau_{\text{im}} > \tau_m$ first and for



$\tau_{\text{im}} < \tau_m$ afterwards. Rearranging the condition $\tau_* < \tau_m$ for the Péclet number reveals the lower bound $27/16 < Pe$ independent of τ_{im}/τ_m . Indeed, the black dotted line for $t_3 = 0$ is vertical in the map (11) for $\tau_{\text{im}} \gg \tau_m$, indicating no dependence on τ_{im}/τ_m in that regime.

So far, we looked at the necessary condition that the lower bound for the interval of the cubic regime is lower than the upper bound. Another approach is to analyse the instantaneous anomalous diffusion exponent $\alpha(t)$. It can be obtained by calculating the slope in a double-logarithmic plot. This is shown in figure E1(c), where α remains close to unity for $t < \tau_*$ and reaches the value three for $\tau_* \ll t \ll \tau_m, \tau_{\text{im}}$. The alternative criterion for the cubic regime to exist is then simply that the maximum value of α_{max} is close to three. With this definition of $\alpha(t)$, superdiffusive parameter regimes are shown with the red colour-coding ranging from one to three in figure 11. This means that the more intense the red in an area is, the closer the parameters are to the asymptotic limits in which the cubic regime emerges. We notice that the red area lies entirely in the region with $t_3 > 0$ and its border follows the same asymptote $Pe^{-1/2}$ for $\tau_m \gg \tau_{\text{im}}$. The cubic regime appears both for $D_{\text{eff}} > D$ and for $D_{\text{eff}} \lesssim D$ for long immobilisations $\tau_{\text{im}} \gg \tau_m$ and for $Pe \gg 1$, as shown in the top right corner of the map in figure 11. For reference, a contour plot of D_{eff}/D is shown in figure H1. The reason for the appearance of the cubic regime regardless of the ratio D_{eff}/D is the existence of the plateau for $\tau_{\text{im}} \gg \tau_m$, which we explain now in detail. We know that regardless of the ratio τ_{im}/τ_m the MSD of initially mobile tracers has the asymptote $2Dt$ for short times $t \ll \tau_m, \tau_{\text{im}}, \tau_v$. In the long-time limit it has the asymptote $2D_{\text{eff}}t$. The MSD of the total density is a strictly monotonic function. This means that if $D_{\text{eff}} < D$, any growth faster than linear must be compensated by a regime with a sublinear growth. This

slower than linear growth arises for long immobilisations only and constitutes the plateau for a sufficiently large ratio $\tau_{\text{im}}/\tau_{\text{m}}$.

I.3. Short immobilisations

Finally, we analyse the case of short immobilisations, $\tau_{\text{im}} \ll \tau_{\text{m}}$. The same series expansion of the total MSD holds as in the case with long immobilisations (27). The difference between the upper and lower bound of the cubic scaling is therefore $t_3 = \tau_{\text{im}} - \tau_{\star}$. Notably, the duration of the cubic regime is shorter as compared to the case with long immobilisations in figure 6(a), because $\tau_{\star} = \sqrt{6D\tau_{\text{m}}/v^2}$ is close to the lower bound τ_{im} for $\tau_{\text{m}} \gg \tau_{\text{im}}$. We emphasise that the cubic regime appears for short immobilisations, whereas for the case without advection the MSD is close to normal, as shown by the grey line in figure 6(b). For $\tau_{\text{im}} \ll \tau_{\text{m}}$, i.e. for negative ordinates in figure H1, the condition $\tau_{\star} \ll \tau_{\text{im}}$ simplifies to $\sqrt{\frac{D}{v^2\tau_{\text{m}}}} = (2\text{Pe})^{-1/2} \ll \sqrt{2/3} \frac{\tau_{\text{im}}}{\tau_{\text{m}}}$. This means that for each ratio $\tau_{\text{im}}/\tau_{\text{m}}$ there exists a lower bound for the Péclet number for the cubic regime to exist. Indeed, the black dotted line on the map in figure II for $t_3 > 0$ has the asymptotic scaling $\text{Pe}^{-1/2}$ for $\tau_{\text{m}} \gg \tau_{\text{im}}$. The cubic regime appears for $t_3 > 0$ only, i.e. only in the top right part from the black dashed line in figure II. In figure II the red colour denotes the maximum anomalous diffusion coefficient α_{max} . The condition $D_{\text{eff}} > 100D$ has the same asymptotic regime $\text{Pe}^{-1/2}$ for $\tau_{\text{m}} \gg \tau_{\text{im}}$, as shown by the black dashed line in figure II. For $\tau_{\text{m}} \gg \tau_{\text{im}}$ the dark red region with α_{max} close to three is almost entirely contained within this region. This means that for $\tau_{\text{m}} \gg \tau_{\text{im}}$ the cubic regime always coexists with $D_{\text{eff}} \gg D$. In contrast, we found that the cubic regime appears regardless of the ratio D_{eff}/D for long immobilisations.

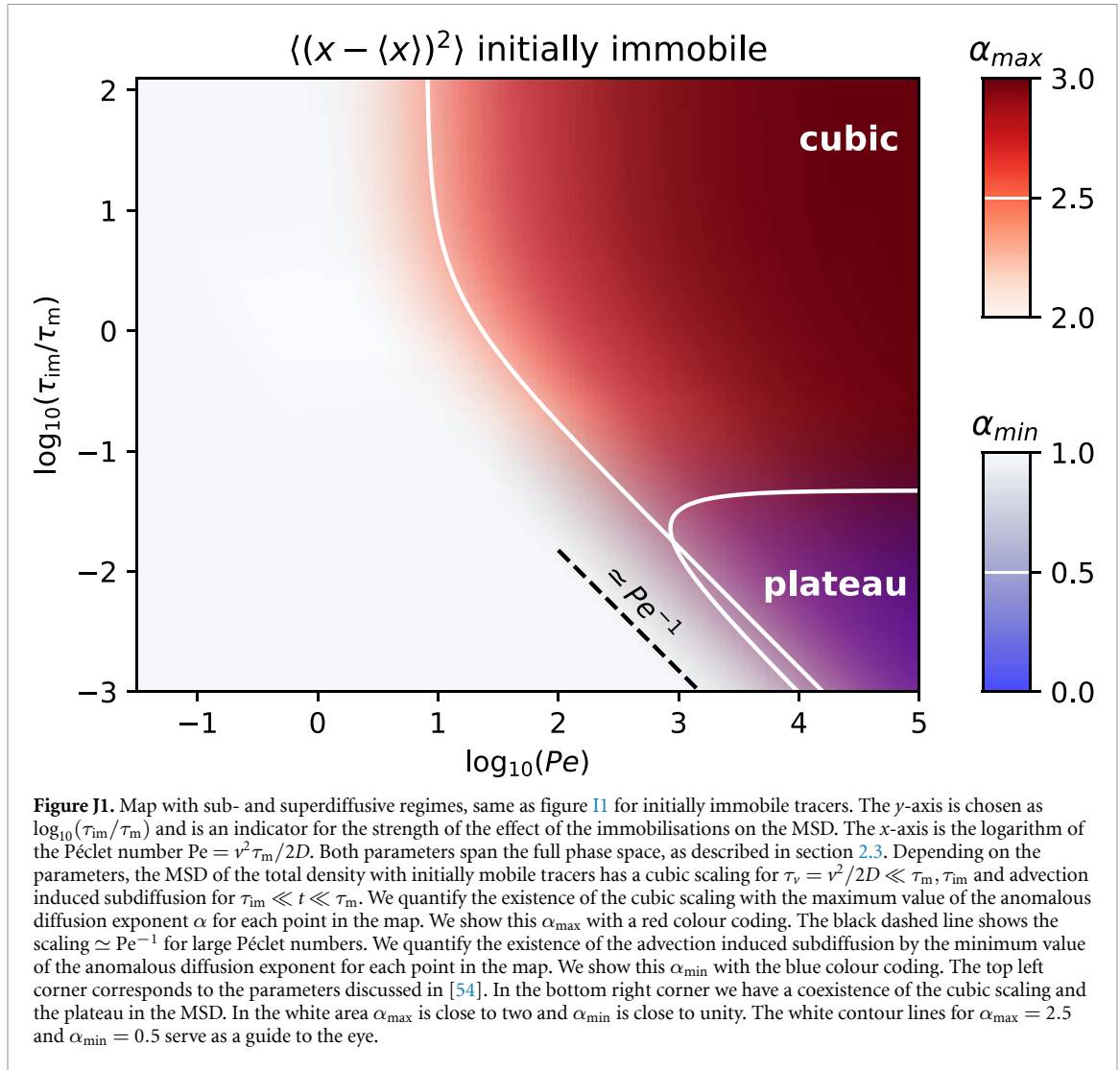
In addition to the maximum value of the instantaneous anomalous diffusion exponent, we consider the minimum value α_{min} in figure II, in which values close to zero correspond to very slow intermediate growth, i.e. a plateau. This allows us to analyse how the plateau at $\tau_{\text{m}} \ll t \ll \tau_{\text{im}}$ is influenced by the presence of advection and the cubic regime. The coexistence of the cubic regime and the plateau can be seen in the MSD in figure 6(a). The top left blue corner in figure II corresponds to the case considered in [54] with long immobilisations and (almost) no advection. The blue subdiffusive area does not significantly change for growing Péclet numbers and it overlaps with the red superdiffusive region in the top right corner of the map in figure II. In the lower left part of figure II(a) white area dominates, in which diffusion is close to normal, with both α_{min} and α_{max} close to unity. This can be seen from the solid grey line in figure 6(b).

Appendix J. Parameter regimes for anomalous diffusion with initially immobile tracers

J.1. Parameter regimes for cubic MSD and advection induced subdiffusion

In section 4.3 we found an anomalous scaling of the MSD, and now we analyse for which values of the Péclet number and the characteristic time scales the cubic scaling of the MSD (35) emerges at intermediate times. The cubic term dominates for $\tau_{\text{v}} \ll t \ll \tau_{\text{m}}, \tau_{\text{im}}$. This implies the time scale separation $\tau_{\text{v}} \ll \tau_{\text{m}}, \tau_{\text{im}}$. For long immobilisations $\tau_{\text{im}} \gg \tau_{\text{m}}$ the parameter space for the cubic scaling to occur is therefore restricted to $\text{Pe} \gg 1$. This can be seen in figure J1 in the top right corner, where we show the decadic logarithm of the Péclet number as the abscissa and $\log_{10}(\tau_{\text{im}}/\tau_{\text{m}})$ as the ordinate. The red colour coding denotes the maximal anomalous diffusion coefficient, which is close to three in that top right region. For clarity, the contour line for $\alpha_{\text{max}} = 2.5$ is shown. For short immobilisations, $\tau_{\text{im}} \ll \tau_{\text{m}}$, the cubic term in the asymptote (35) dominates for $\tau_{\text{v}} \ll t \ll \tau_{\text{im}}$, which limits the parameter space for the cubic scaling to occur to $\frac{\tau_{\text{im}}}{\tau_{\text{m}}} \gg \text{Pe}^{-1}$. This can be seen in the map in figure J1, where the relation $\frac{3}{2}\text{Pe}^{-1} \ll \frac{\tau_{\text{im}}}{\tau_{\text{m}}}$ is shown as a dashed black line. Below this line no cubic scaling is possible, meaning that for a given Péclet number the fraction $\tau_{\text{m}}/\tau_{\text{im}}$ needs to be sufficiently small.

After the cubic scaling an advection induced subdiffusion regime may emerge. The time-domain of the subdiffusion is given by $\tau_{\text{v}} \ll \tau_{\text{im}} \ll t \ll \tau_{\text{m}}$. Therefore, the subdiffusive regime appears only for short immobilisations, $\tau_{\text{im}} \ll \tau_{\text{m}}$. Furthermore, the condition $\tau_{\text{v}} \ll \tau_{\text{im}}$ translates to $\text{Pe}^{-1} \ll \tau_{\text{im}}/\tau_{\text{m}}$, shown as the dotted line in figure J1. This restricts the parameter space for the plateau. It is bound by $\tau_{\text{im}} \ll \tau_{\text{m}}$, corresponding to the horizontal boundary in figure J1. In the map in figure J1 we show α_{min} for the total MSD as a blue colour map and observe a region with $\alpha_{\text{min}} < 1/2$ in the bottom right corner for a high Péclet number and short immobilisations. As a guide to the eye we show a contour line for $\alpha_{\text{min}} = 1/2$. A corresponding MSD is shown in figure 9(b), where a plateau occurs for $\tau_{\text{im}} \ll t \ll \tau_{\text{m}}$. This is a new behaviour that does not occur in the case without advection, as is shown by the grey line in figure J1 for a small Péclet number.



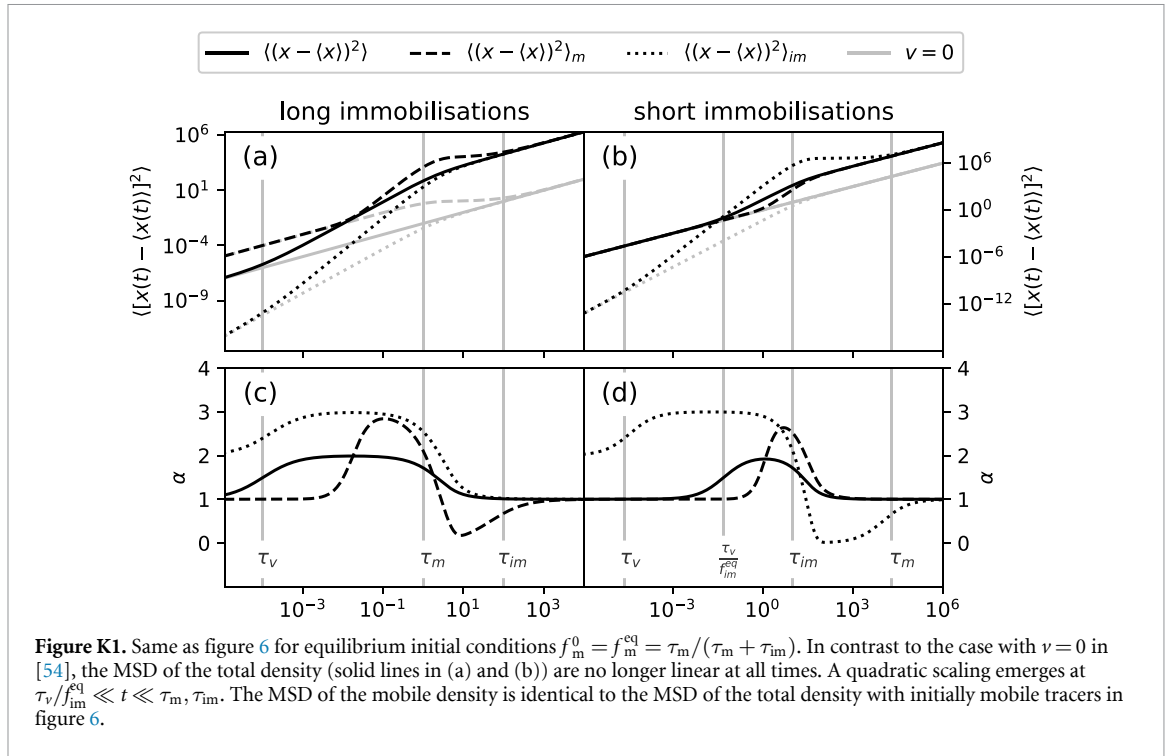
Appendix K. Equilibrium initial condition

We assume the equilibrium fractions $f_m^0 = f_m^{eq} = \tau_m / (\tau_m + \tau_{im})$ and $f_{im}^0 = f_{im}^{eq} = \tau_{im} / (\tau_m + \tau_{im})$ and consider the MSD of the total density. It is shown in figures K1(a) and (b) as the solid black line for long and short immobilisations, respectively. The densities are given by adding the densities for mobile and immobile initial conditions with the corresponding equilibrium fractions as factors. The MSD is not a linear function and does not follow a linear combination of the initially mobile and immobile MSDs. In contrast to the case without advection in [54], the MSD is no longer linear at all times, and we observe a quadratic scaling for $\tau_v(\tau_m + \tau_{im})/\tau_{im} \ll t \ll \tau_m, \tau_{im}$. A series expansion yields the asymptote for intermediate times $t \ll \tau_m, \tau_{im}$, where t can be shorter or longer than τ_v ,

$$\langle [x(t) - \langle x(t) \rangle]^2 \rangle \sim 2Df_m^{eq}t + v^2f_m^{eq}f_{im}^{eq}t^2, \text{ for } t \ll \tau_m, \tau_{im}. \quad (\text{K.1})$$

The quadratic term dominates over the linear term for $\frac{\tau_v}{f_{im}^{eq}} \ll t$. This is shown in figures K1(a) and (b). In panels (c) and (d) the instantaneous anomalous diffusion exponent is displayed, which is close to two in this domain. Note that for long immobilisations $f_{im}^{eq} \approx 1$. The quadratic scaling emerges for long immobilisations $\tau_m \ll \tau_{im}$ for $Pe \gg 1$ and for short immobilisations for $Pe^{-1/2} \ll \tau_{im}/\tau_m$.

As described in [54], the MSD of the mobile density with equilibrium initial conditions is identical to the MSD of the total density with mobile initial conditions. We discussed this case in detail in the main text. The same holds for the MSD of the immobile density. For an equilibrium fraction of initially mobile tracers the density is given by the linear combination of the results for mobile and for immobile initial conditions.



Appendix L. Comparison to CTRW

In this section we compare our results to three versions of CTRWs. For didactic purposes, we start in appendix L.1 with the classical CTRW with exponentially distributed waiting times. In appendix L.2 we compare our model to the two state CTRW [51]. Finally, in appendix L.3 we compare our model to a CTRW in which the waiting times are drawn from a waiting time distribution containing two exponential distributions [52].

L.1. Classical CTRW

We here compare the results obtained from the MIM (3) to a CTRW with advection and exponentially distributed sojourn times. The relation between MIM and CTRW has been discussed in detail, for example, in [13, 48, 70]. Let us define the sojourn time density $\psi(t) = \exp(-t/\tau)/\tau$ and the Gaussian displacement density $\lambda(x)$ with mean μ and variance σ^2 . This corresponds to the model considered in [46]. In [71] the solution of the density function $p(x, t)$ in this CTRW framework is given as

$$p(x, t) = \sum_{j=1}^{\infty} \frac{(t/\tau)^j \exp(-t/\tau)}{j!} \frac{\exp\left(-\frac{x^2}{2j\sigma^2}\right)}{\sqrt{2\pi j\sigma^2}}, \tag{L.1}$$

for $\mu = 0$. We incorporate the non-zero mean μ and obtain the solution

$$p(x, t) = \sum_{j=1}^{\infty} \frac{(t/\tau)^j \exp(-t/\tau)}{j!} \frac{\exp\left(-\frac{(x-j\mu)^2}{2j\sigma^2}\right)}{\sqrt{2\pi j\sigma^2}}. \tag{L.2}$$

Let us turn to the moments of $p(x, t)$ (L.2). The first moment is given by

$$\begin{aligned} \langle x(t) \rangle &= \sum_{j=1}^{\infty} \frac{(t/\tau)^j \exp(-t/\tau)}{j!} j\mu \\ &= \mu \frac{t}{\tau} \exp\left(-\frac{t}{\tau}\right) \sum_{j=0}^{\infty} \frac{(t/\tau)^j}{j!} \\ &= \mu \frac{t}{\tau}. \end{aligned} \tag{L.3}$$

In the same way we obtain the second moment

$$\langle x^2(t) \rangle = \sigma^2 \frac{t}{\tau} + \mu^2 \frac{t^2}{\tau^2} + \mu^2 \frac{t}{\tau}, \quad (\text{L.4})$$

resulting in the MSD

$$\langle [x(t) - \langle x(t) \rangle]^2 \rangle = \frac{\sigma^2}{\tau} t + \frac{\mu^2}{\tau} t, \quad (\text{L.5})$$

which is linear at all times, in contrast the results obtained from our model.

L.2. Two-state CTRW

In this section we compare our model to the two-state CTRW introduced in [51] in which two transition densities

$$f_i(x, t) = \frac{1}{\sqrt{4\pi D_i t}} \exp\left(-\frac{(x - v_i t)^2}{4D_i t}\right) \psi_i(t), \quad i = 1, 2 \quad (\text{L.6})$$

are present with average speeds v_i and diffusion constants D_i . In an alternating way jumps are drawn from $f_1(x, t)$ and $f_2(x, t)$. The long-time diffusion coefficient presented in [51] is given by

$$D_{\text{eff}} = \frac{D_1 \tau_1 + D_2 \tau_2}{\tau_1 + \tau_2} + \frac{1}{2(\tau_1 + \tau_2)} \times \left[\sigma_1^2 \left(v_1 - \frac{v_1 \tau_1 + v_2 \tau_2}{\tau_1 + \tau_2} \right) + \sigma_2^2 \left(v_2 - \frac{v_1 \tau_1 + v_2 \tau_2}{\tau_1 + \tau_2} \right) \right] \quad (\text{L.7})$$

with $\tau_i = \int_0^\infty t \psi_i(t) dt$ and $\sigma_i^2 = \int_0^\infty t^2 \psi_i(t) dt - \tau_i^2$, $i = 1, 2$. The long-time effective diffusion coefficient (L.7) matches our result (15), if we formally choose $D_1 = D$, $v_1 = v$, $D_2 = 0$, $v_2 = 0$, $\psi_1(t) = \exp(-t/\tau_m)/\tau_m$ and $\psi_2(t) = \exp(-t/\tau_{\text{im}})/\tau_{\text{im}}$.

L.3. Double exponential CTRW

In this section we compare our model to the CTRW analysed in [52], in which the waiting time distribution function is given by the weighted sum

$$\psi(t) = \frac{p}{\tau_D} \exp\left(-\frac{t}{\tau_D}\right) + \frac{(1-p)}{\tau_B} \exp\left(-\frac{t}{\tau_B}\right) \quad (\text{L.8})$$

of two exponentials, where $\tau_B \leq \tau_D$ and $p \in [0, 1]$. The jump length distribution we consider is given by the Gaussian

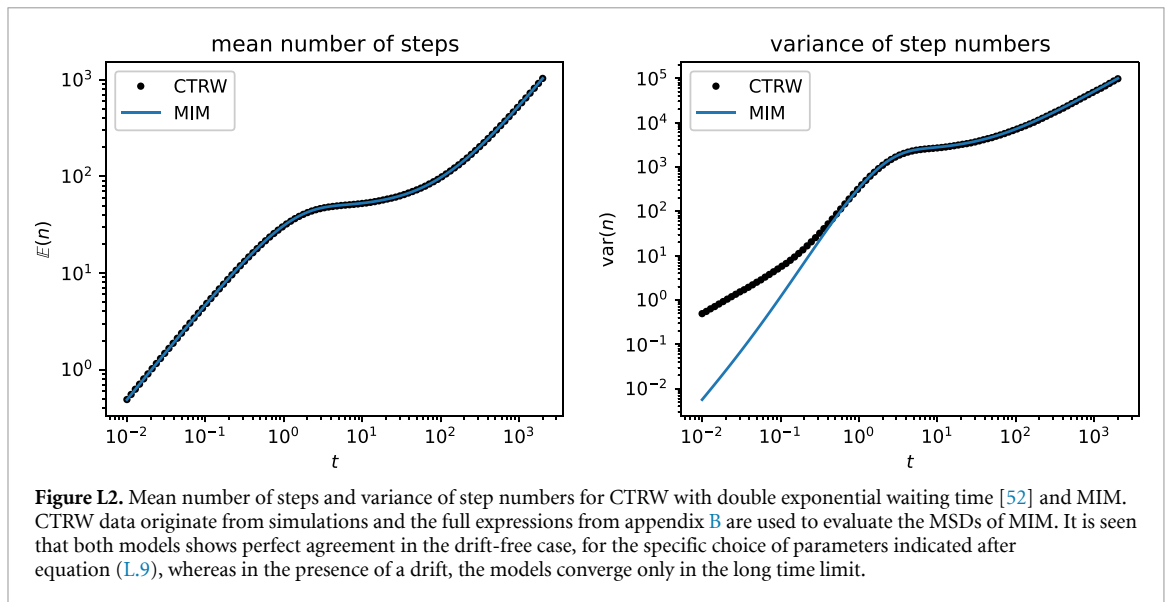
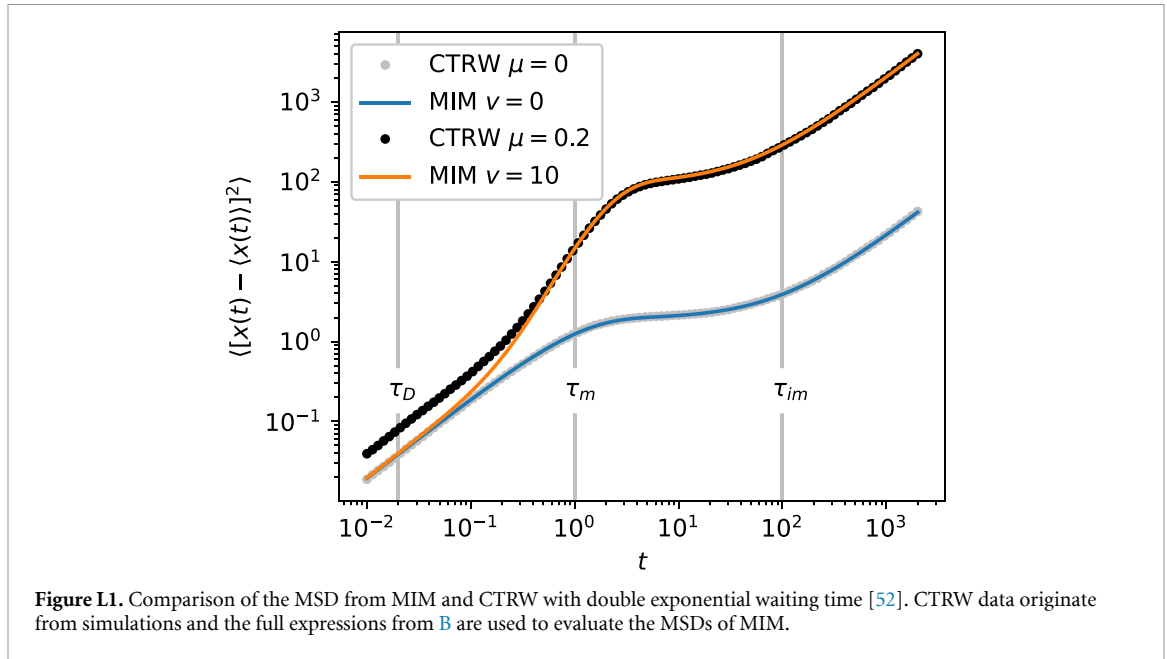
$$\lambda(x) = \frac{1}{\sqrt{2\pi\sigma^2}} \exp\left(-\frac{(x-\mu)^2}{2\sigma^2}\right), \quad (\text{L.9})$$

with mean μ and variance σ^2 . Note that in [52] $\lambda(x)$ is restricted to the case $\mu = 0$. Formally, we choose the parameters $\tau_B = \tau_{\text{im}}$, $\tau_D \ll \tau_B, \tau_{\text{im}}$, and $p = 1 - \tau_D/\tau_m$. We stress that this means that $\tau_D \neq \tau_m$ and τ_D does not have the meaning of the mean residence time in a mobile state. By choosing $\tau_D \ll \tau_m$ and $p = 1 - \tau_D/\tau_m$ close to unity there is a high probability to draw from the exponential distribution with short mean duration. This effectively models the Brownian motion of a tracer in the mobile state. After each step, the tracer immobilises with probability $1 - p$. If there was no waiting time drawn from the long exponential, on average, there are t/τ_D steps at time t . This gives an effective immobilisation rate of $1/\tau_m$, which is the same as in MIM. In figure L1 we compare the MSD of MIM for $\tau_m = 1$, $\tau_{\text{im}} = 100$, $v = 0$ or $v = 10$ and $D = 1$ with simulations of CTRW with $\tau_D = 2 \times 10^{-2}$, $\tau_B = \tau_{\text{im}}$, $\mu = v\tau_D$ and $\sigma = \sqrt{2D\tau_D}$. We find good agreement at all times for the advection-free case, while the CTRW yields higher values than MIM for $t < \tau_D$ in the case with advection.

The reason why the MSDs are identical in the advection-free case and not in the case with advection can be understood by considering the MSD in terms of step numbers n [66]

$$\text{var}(x) = \mathbb{E}(n) \text{var}(\Delta x_i) + (\mathbb{E}(\Delta x_i))^2 \text{var}(n), \quad (\text{L.10})$$


where $x = \sum_{i=1}^n \Delta x_i$, as introduced in section 2.5. We emphasise that expression (L.10) is exact. From expression (L.10) we see that in the advection-free case $\mathbb{E}(\Delta x_i) = 0$ only the mean number of steps is relevant for the MSD and not the variance of step numbers. Indeed, in figure L2 we show the mean number



of steps $\mathbb{E}(n)$ (calculated by setting $D=0$), where the dots for CTRW and the line for MIM overlap at all times. Therefore, the MSDs in the advection-free case of CTRW and MIM in figure L1 are equivalent. In contrast, in the case of advection, the variance of step numbers $\text{var}(n)$ couples to the MSD, as can be seen in expression (L.10). The variance of step numbers differs for $t < \tau_D$. We explain this as follows. If a tracer is in the mobile state of MIM, it will have a fixed number of steps $n = t/\Delta t$ at time t . The stochasticity of step numbers arises solely from immobilisations. By setting $D=0$ we obtain a cubic short-time growth of the variance from the short-time asymptote (27). In contrast, in the CTRW case, the number of steps is random even in the case of a simple CTRW with only one exponential waiting time distribution, as described in appendix L.1. It can be seen in the variance of CTRW (L.5) for $\sigma = 0$ and $\mu = 1$, where the variance of step numbers grows linearly. This is due to the fact that after each step a random waiting time is drawn from the exponential distribution. Therefore, the variance of step numbers is higher for small times and hence the MSDs of MIM and CTRW do not overlap for $t < \tau_D$, as shown in figure L1. We point out that the disagreement between the MSD of MIM and CTRW with advection lasts until $\approx 3 \times 10^{-1}$, which is notably larger than the chosen $\tau_D = 2 \times 10^{-2}$.

ORCID iDs

Ralf Metzler  <https://orcid.org/0000-0002-6013-7020>

Aleksei V Chechkin  <https://orcid.org/0000-0002-3803-1174>

References

- [1] Biggar J W and Nelson D R 1967 Miscible displacement and leaching phenomena *Irrigation of Agricultural Lands (Agronomy)* vol 11 (Madison, WI: American Society of Agronomy), ed R M Hagen p 254
- [2] Lapidus L and Amundson N R 1952 Mathematica of adsorption in beds. VI. the effect of longitudinal diffusion in ion exchange and chromatographic columns *J. Phys. Chem.* **56** 984
- [3] Coats K H and Smith B D 1964 Dead-end pore volume and dispersion in porous media *Soc. Pet. Eng. J.* **4** 73
- [4] Van Genuchten M T and Wierenga P J 1976 Mass transfer studies in sorbing porous media I. Analytical solutions *Soil Sci. Soc. Am. J.* **40** 473
- [5] Doerries T J, Chechkin A V, Schumer R and Metzler R 2022 Rate equations, spatial moments and concentration profiles for mobile-immobile models with power-law and mixed waiting time distributions *Phys. Rev. E* **105** 014105
- [6] Michalak A M and Kitanidis P K 2000 Macroscopic behavior and random-walk particle tracking of kinetically sorbing solutes *Water Resour. Res.* **36** 2133
- [7] Goltz M N and Tobrtyd P V 1987 Using the method of moments to analyse three-dimensional diffusion-limited solute transport from temporal and spatial perspectives *Water Resour. Res.* **23** 1575
- [8] van Genuchten M T and Wierenga P J 1976 Mass transfer studies in sorbing porous media I. Analytical solutions *Soil Sci. Soc. Am. J.* **40** 473
- [9] Deans H H 1963 A mathematical model for dispersion in the direction of flow of porous media *Soc. Pet. Eng. J.* **3** 49
- [10] Sardin M, Schweich D, Leij F J and van Genuchten M T 1991 Modeling the nonequilibrium transport of linearly interacting solutes in porous media: a review *Water Resour. Res.* **27** 2287
- [11] Haggerty R and Gorelick S M 1995 Multiple-rate mass transfer for modeling diffusion and surface reactions in media with pore-scale heterogeneity *Water Resour. Res.* **31** 2383
- [12] Schumer R, Benson D A, Meerschaert M M and Baeumer B 2003 Fractal mobile-immobile solute transport *Water Resour. Res.* **39** 1296
- [13] Dentz M and Berkowitz B 2003 Transport behavior of a passive solute in continuous time random walks and multirate mass transfer *Water Resour. Res.* **39** 1
- [14] Zhang Y, Benson D A and Baeumer B 2008 Moment analysis for spatiotemporal fractional dispersion *Water Resour. Res.* **44** W04424
- [15] Gao G, Zhan H, Feng S, Fu B, Ma Y and Huang G 2010 A new mobile-immobile model for reactive solute transport with scale-dependent dispersion *Water Resour. Res.* **46** W08533
- [16] Lu B, Zhang Y, Zheng C, Green C T, O'Neill C, Sun H-G and Qian J 2018 Comparison of time nonlocal transport models for characterizing non-Fickian transport: from mathematical interpretation to laboratory application *Water* **10** 778
- [17] Egusa N, Nakagawa K and Hirata T 2020 A retardation factor considering solute transfer between mobile and immobile water in porous media *Environ. Model. Assess.* **26** 103
- [18] Goepfert N, Goldscheider N and Berkowitz B 2020 Experimental and modeling evidence of kilometer-scale anomalous tracer transport in an alpine karst aquifer *Water Res.* **178** 115755
- [19] Weigel A V, Simon B, Tamkun M M and Krapf D 2011 Ergodic and nonergodic processes coexist in the plasma membrane as observed by single-molecule tracking *Proc. Natl Acad. Sci. USA* **108** 6438
- [20] Pulkkinen O and Metzler R 2013 Distance matters: the impact of gene proximity in bacterial gene regulation *Phys. Rev. Lett.* **110** 198101
- [21] Igaev M, Janning D, Sündermann F, Niewidok B, Brandt R and Junge W 2014 A refined reaction-diffusion model of tau-microtubule dynamics and its application in FDAP analysis *Biophys. J.* **107** 2567
- [22] Janning D, Igaev M, Sündermann F, Brühmann J, Beutel O, Heinisch J J, Bakota L, Piehler J, Junge W and Brandt R 2014 Single-molecule tracking of tau reveals fast kiss-and-hop interaction with microtubules in living neurons *Mol. Biol. Cell* **25** 3541
- [23] Yeung C, Shtrahman M and Wu X-L 2007 Stick-and-diffuse and caged diffusion: a comparison of two models of synaptic vesicle dynamics *Biophys. J.* **92** 2271
- [24] Wu M M, Covington E D and Lewis R S 2014 Single-molecule analysis of diffusion and trapping of STIM1 and Orai1 at endoplasmic reticulum-plasma membrane junctions *Mol. Biol. Cell* **25** 3672
- [25] Fernández A D, Charchar P, Cherstvy A G, Metzler R and Finnis M W 2020 The diffusion of doxorubicin drug molecules in silica nanoslits is non-Gaussian, intermittent and anticorrelated *Phys. Chem. Chem. Phys.* **22** 27955
- [26] van den Broek B, Lomholt M A, Kalisch S-M J, Metzler R and Wuite G J L 2008 How DNA coiling enhances target localization by proteins *Proc. Natl Acad. Sci.* **105** 15738
- [27] Mazza D, Abernathy A, Golob N, Morisaki T and McNally J G 2012 A benchmark for chromatin binding measurements in live cells *Nucleic Acids Res.* **40** e119
- [28] Liu Z, Legant W R, Chen B-C, Li L, Grimm J B, Lavis L D, Betzig E and Tjian R 2014 3D imaging of Sox2 enhancer clusters in embryonic stem cells *eLife* **3** e04236
- [29] Sprague B L, Pego R L, Stavreva D A and McNally J G 2004 Analysis of binding reactions by fluorescence recovery after photobleaching *Biophys. J.* **86** 3473
- [30] Chen J *et al* 2014 Single-molecule dynamics of enhanceosome assembly in embryonic stem cells *Cell* **156** 1274
- [31] Park S, Lee O-C, Durang X and Jeon J-H 2021 A mini-review of the diffusion dynamics of DNA-binding proteins: experiments and models *J. Korean Phys. Soc.* **78** 408
- [32] Tafvizi A, Mirny L A and van Oijen A M 2011 Dancing on DNA: kinetic aspects of search processes on DNA *ChemPhysChem* **12** 1418
- [33] Tafvizi A, Huang F, Fersht A R, Mirny L A and van Oijen A M 2011 A single-molecule characterization of p53 search on DNA *Proc. Natl Acad. Sci. USA* **108** 563
- [34] Kong M *et al* 2016 Single-molecule imaging reveals that Rad4 employs a dynamic DNA damage recognition process *Mol. Cell* **64** 376

- [35] Kamagata K, Mano E, Ouchi K, Kanabayashi S and Johnson R C 2018 High free-energy barrier of 1D diffusion along DNA by architectural DNA-binding proteins *J. Mol. Biol.* **430** 655
- [36] Revere J F, Jeon J-H, Bao H, Leippe M, Metzler R and Selhuber-Unkel C 2015 Superdiffusion dominates intracellular particle motion in the supercrowded cytoplasm of pathogen *Acanthamoeba castellanii* *Sci. Rep.* **5** 11690
- [37] Wang L and Li P C H 2011 Microfluidic DNA microarray analysis: a review *Anal. Chim. Acta* **687** 12
- [38] Squires T M, Mesinger R J and Manalis R 2008 Making it stick: convection, reaction and diffusion in surface-based biosensors *Nat. Biotechnol.* **26** 417
- [39] Scher H and Montroll E W 1975 Anomalous transient-time dispersion in amorphous solids *Phys. Rev. B* **12** 2455
- [40] Kurilovich A A, Mantsevich V N, Mardoukhi Y, Stevenson K J, Chechkin A V and Palyulin V V 2022 Non-Markovian diffusion of excitons in layered perovskites and transition metal dichalcogenides *Phys. Chem. Chem. Phys.* **24** 13941
- [41] Kurilovich A A, Mantsevich V N, Stevenson K J, Chechkin A V and Palyulin V V 2020 Complex diffusion-based kinetics of photoluminescence in semiconductor nanoplatelets *Phys. Chem. Chem. Phys.* **22** 24686
- [42] Kurilovich A A, Mantsevich V N, Stevenson K J, Chechkin A V and Palyulin V V 2021 Trapping-influenced photoluminescence intensity decay in semiconductor nanoplatelets *J. Phys.: Conf. Ser.* **2015** 012103
- [43] Harvey C F and Gorelick S M 1995 Temporal moment-generating equations: modeling transport and mass transfer in heterogeneous aquifers *Water Resour. Res.* **31** 1895
- [44] Hughes B D 1995 *Random Walks and Random Environments: Random Walks* vol 1 (Oxford: Oxford University Press)
- [45] Montroll E W and Weiss G H 1965 Random walks on lattices. II *J. Math. Phys.* **6** 167
- [46] Burov S, Wang W and Barkai E 2022 Exponential tails and asymmetry relations for the spread of biased random walks, (arXiv:2209.03410)
- [47] Edery Y, Guadagnini A, Scher H and Berkowitz B 2014 Origins of anomalous transport in heterogeneous media: structural and dynamic controls *Water Resour. Res.* **50** 1490
- [48] Margolin G, Dentz M and Berkowitz B 2003 Continuous time random walk and multirate mass transfer modeling of sorption *Chem. Phys.* **295** 71
- [49] Krüsemann H, Godec A and Metzler R 2014 First-passage statistics for aging diffusion in systems with annealed and quenched disorder *Phys. Rev. E* **89** 040101(R)
- [50] Berkowitz B, Klafter J, Metzler R and Scher H 2002 Physical pictures of transport in heterogeneous media: advection-dispersion, random-walk and fractional derivative formulations *Water Resour. Res.* **38** 1191
- [51] Weiss G H 1976 The two-state random walk *J. Stat. Phys.* **15** 157
- [52] Vitali S, Paradisi P and Pagnini G 2022 Anomalous diffusion originated by two Markovian hopping-trap mechanisms *J. Phys. A: Math. Theor.* **55** 224012
- [53] Hidalgo-Soria M, Barkai E and Burov S 2021 Cusp of non-Gaussian density of particles for a diffusing diffusivity model *Entropy* **23** 231
- [54] Doerries T J, Chechkin A V and Metzler R 2022 Apparent anomalous diffusion and non-Gaussian distributions in a simple mobile-immobile transport model with Poissonian switching *J. R. Soc. Interface* **19** 20220233
- [55] Gouze P, Le Borgne T, Leprovost R, Lods G, Poidras T and Pezard P 2008 Non-Fickian dispersion in porous media: 1. Multiscale measurements using single-well injection withdrawal tracer tests *Water Resour. Res.* **44** W06426
- [56] Drummond J D, Larsen L G, González-Pinzón R, Packman A I and Harvey J W 2017 Fine particle retention within stream storage areas at base flow and in response to a storm event *Water Resour. Res.* **53** 5690–705
- [57] Metzler R, Rajyaguru A and Berkowitz B 2022 Modelling anomalous diffusion in semi-infinite disordered systems and porous media *New J. Phys.* **24** 123004
- [58] Metzler R and Klafter J 2000 The random walk's guide to anomalous diffusion: a fractional dynamics approach *Phys. Rep.* **339** 1
- [59] Bochner S 1960 *Harmonic Analysis and the Theory of Probability* (Berkeley, CA: Berkeley University Press)
- [60] Chechkin A V, Seno F, Metzler R and Sokolov I M 2017 Brownian yet non-Gaussian diffusion: from superstatistics to subordination of diffusing diffusivities *Phys. Rev. X* **7** 021002
- [61] Chechkin A and Sokolov I M 2021 Relation between generalized diffusion equations and subordination schemes *Phys. Rev. E* **103** 032133
- [62] Gorenflo R and Mainardi F 2009 Some recent advances in theory and simulation of fractional diffusion processes *J. Comput. Appl. Math.* **229** 400
- [63] Fogedby H C 1994 Langevin equations for continuous time Lévy flights *Phys. Rev. E* **50** 1657
- [64] Eule S and Friedrich R 2009 Subordinated Langevin equations for anomalous diffusion in external potentials – biasing and decoupled external forces *Europhys. Lett.* **86** 30008
- [65] Gorenflo R, Mainardi F and Vivoli A 2007 Continuous-time random walk and parametric subordination in fractional diffusion *Chaos Solitons Fractals* **34** 87
- [66] Ross S M 2010 *A First Course in Probability* vol 8, ed D Lynch (London: Pearson) p 362
- [67] Muñoz-Gil G et al 2021 Objective comparison of methods to decode anomalous diffusion *Nat. Commun.* **12** 6253
- [68] Seckler H and Metzler R 2022 Bayesian deep learning for error estimation in the analysis of anomalous diffusion *Nat. Commun.* **13** 6717
- [69] Manzo C, Muñoz-Gil G, Volpe G, Garcia-March M A, Lewenstein M and Metzler R 2023 Preface: characterisation of physical processes from anomalous diffusion data *J. Phys. A* **56** 010401
- [70] Boano F, Packman A I, Cortis A, Revelli R and Ridolfi L 2007 A continuous time random walk approach to the stream transport of solutes *Water Resour. Res.* **43** 1
- [71] Barkai E and Burov S 2020 Packets of diffusing particles exhibit universal exponential tails *Phys. Rev. L* **124** 060603